Philipp Raggam, BSc

Towards a passive Brain-Computer Interface for Mental State Monitoring

Master's Thesis

to achieve the university degree of

Master of Science

Master's degree programme: Biomedical Engineering

submitted to

Graz University of Technology

Supervisor

Ass.Prof. Priv.-Doz. Mag.rer.nat. Dr.phil. Selina Christin Wriessnegger

Institute of Neural Engineering
Head: Univ.-Prof. Dipl-Ing. Dr.techn. Gernot Müller-Putz

Graz, May 2020

Affidavit

I declare that I have authored this thesis independently, that I have not used other than the declared sources/resources, and that I have explicitly indicated all material which has been quoted either literally or by content from the sources used. The text document uploaded to TUGRAZonline is identical to the present master's thesis.

Date	Signature

Acknowledgements

I would like express my gratitude first and foremost to my supervisor, Ass.Prof. Priv.-Doz. Mag.rer.nat. Dr.phil. Selina Christin Wriessnegger, who suggested this topic, provided useful ideas and feedback, and always took time to answer my questions. I would also like to thank Joana Pereira M.Sc. and Dipl.-Ing. Andreas Schwarz, whose assistance was essential for the completion of this thesis. Furthermore, I want to thank Univ.-Prof. Dipl-Ing. Dr.techn. Gernot Müller-Putz for enabling this thesis and all the colleagues from the Institute of Neural Engineering for their support.

I would like to address my thanks to all the participants, who willingly shared their time and energy to take part in my study. Last but not least, I want to express my gratitude to my family and friends, for their support and encouragement throughout my studies.

Abstract

With increasing developments of modern technologies like artificial intelligence and virtual reality environments, more and more applications make use of mental state monitoring systems. These systems allow applications to be adapted based on the user's mental state and are applied in various fields like driving or teaching assistance. This thesis aims towards the development of a passive Brain-Computer Interface for mental state monitoring. The goal was to implement an algorithm to detect high mental workload and fatigue in participants while performing a cognitive demanding task. As a first step, band power features in the theta and alpha frequency band of the EEG were inspected. The band power changes over time were analysed at different task conditions and cortical areas. To support the findings of the band power changes, subjective ratings (questionnaires concerning fatigue and workload levels) and behavioural measures (performance accuracies and response times) were considered. The detection of high mental workload and fatigue was implemented by applying the Riemannian geometry on the band power features of the EEG. Mental workload and fatigue were considered as too high, when the Riemannian distances of the task-run EEG reached or surpassed the threshold of the baseline EEG. The results showed an increase of the band power in the theta and alpha frequency bands over time, which is associated with increasing mental workload and fatigue and correlated to the participant's task performance. In 8 out of the 20 participants, high mental workload and fatigue could be detected, 6 of them belonged to the group with lower task performance. The Riemannian distances also showed a steady increase towards the threshold with increasing experiment duration, with the most detections occurring at the last run of the experiment.

Keywords: EEG, passive BCI, mental workload and fatigue, band power features, Riemannian geometry

Kurzfassung

Moderne technologische Anwendungen machen immer mehr Gebrauch von Systemen zur Überwachung des mentalen Zustands ihrer Benutzer. Solche Systeme ermöglichen die Adaptierung von Anwendungen basierend auf den Änderungen des mentalen Zustands, und werden in verschiedenen Bereichen wie Fahr- oder Lernassistenz eingesetzt. Diese Arbeit zielt auf die Entwicklung einer passiven Hirn-Computer-Schnittstelle zur Überwachung des mentalen Zustands ab. Ziel war es, einen Algorithmus zu entwickeln, der eine hohe mentale Auslastung und Ermüdung der Benutzer bei der Ausführung einer kognitiv anspruchsvollen Aufgabe erkennt. Hierzu wurde die Bandpower der neuronalen Aktivität im Theta- und Alpha-Frequenzband des EEGs untersucht. Die zeitliche Änderung der Bandpower wurde bei verschiedenen Aufgabenschwierigkeiten und kortikalen Arealen analysiert. Die Ergebnisse wurden mit Fragebögen und Aufgabenerfüllung untermauert. Die Detektion von hoher mentaler Auslastung und Ermüdung wurde mittels der Riemannschen Geometrie umgesetzt. Mentale Auslastung und Ermüdung wurden als zu hoch erkannt, wenn die Riemannschen Abstände des EEGs während der Aufgabenausführung die Schwelle des Ruhe-EEGs erreichten oder überstiegen. Die Ergebnisse zeigten einen Anstieg der Bandpower im Theta- und Alpha-Frequenzband mit zunehmender Experimentdauer, was mit steigender mentaler Auslastung und Ermüdung einhergeht. Bei 8 der 20 Teilnehmer konnte eine hohe mentale Auslastung und Ermüdung festgestellt werden, 6 von ihnen gehörten zur Gruppe mit geringerer Aufgabenerfüllung. Die Riemannschen Abstände zeigten mit zunehmender Experimentdauer eine stetige Zunahme Richtung Schwellwert, mit den meisten Detektionen im letzten Versuchsdurchlauf.

Schlüsselwörter: EEG, passive Hirn-Computer-Schnittstelle, mentale Auslastung und Ermüdung, Bandpower, Riemannsche Geometrie

Contents

List of Figures

List of Tables

1 Introduction

The first chapter introduces Brain-Computer Interfaces (BCIs) by describing their different stages and categories, together with their brain signal acquisition techniques. The basic principles of the electroencephalography (EEG) and the different brain signal types are explained in more detail. Furthermore, the terms of mental workload (MWL) and mental fatigue (MF) are defined, as well as their connections to BCIs and the EEG. At the end of this chapter, the aim of the thesis and the hypothesis are stated.

1.1 Basic Principles of BCIs

> **"A brain-computer interface is a device that does not use the normal neuromuscular output pathways of the brain, but accepts commands encoded in neuro-physiological signals."**
>
> **John Wolpaw, 1991**

A BCI is a system, which bypasses the natural output of the central nervous system (CNS) by translating the user's intentions into commands for communication or locomotion control [1], [2]. In order to translate the user's intentions into commands, this system monitors, processes and decodes brain signals and converts them into control signals for application interfaces [3]. The individual stages of a BCI system are shown in Figure 1.1 and can be described as follows [4]:

- **Signal acquisition:** At this stage, the brain signals are monitored, the analogue signals converted into digital signals and preprocessing is applied on the data (noise and artefact reduction).

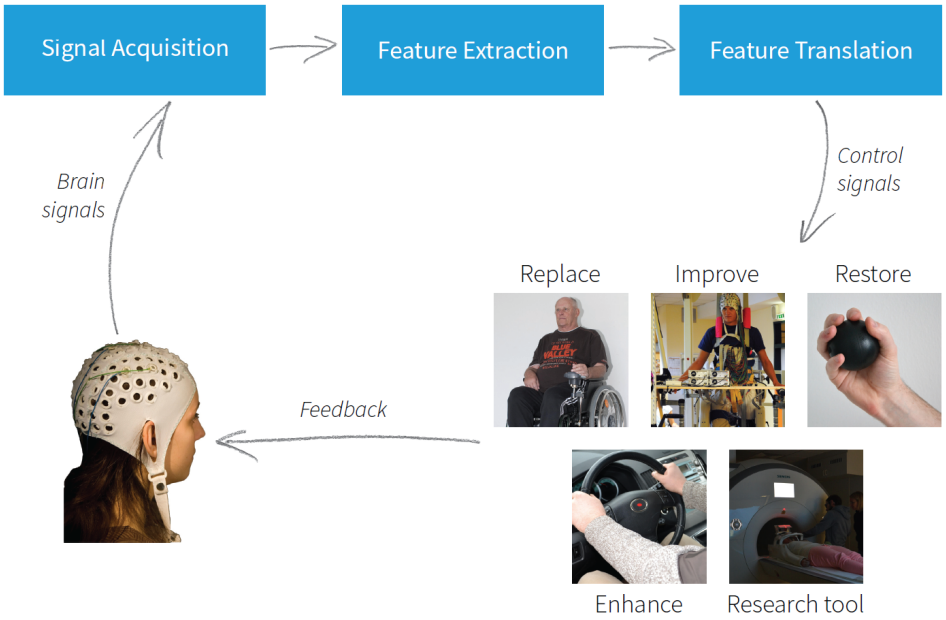

Figure 1.1: Stages of a BCI system: Signal acquisition, feature extraction, feature translation and application interface (adapted from Wolpaw et al. [4]).

- **Feature extraction:** Further signal processing methods are applied to extract representative and discriminable features from the brain signals (such as signal amplitude or frequency).
- **Feature translation:** Classification algorithms are used to assign a certain brain signal feature to a corresponding control signal, or to find patterns in the brain signals.
- **Application interface:** At the last stage, output devices are controlled in order to replace, improve, restore or enhance the natural output of the CNS [5], or use them for research tools and provide feedback for the user.

The utilization of BCIs has already been shown in various applications such as selecting letters from a virtual keyboard [6]–[8], controlling prosthetic devices [9], [10] or in a non-clinical context such as education and entertainment [11]–[13].

1.1.1 BCI Categories

A BCI translates changes of brain signals into commands [7]. These changes are of physiological origin and can be elicited in three different ways - actively, passively and reactively [14], [15]:

- **Active BCIs:** The outputs are derived from brain activity which is directly and consciously controlled by the user. The user actively controls an application, independent of external events, such as spelling devices [6]–[8] or prosthetic devices [9], [10].
- **Reactive BCIs:** The outputs are derived from brain activity which arises in reaction to external stimulation. The user controls an application by indirectly modulating its brain activity.
- **Passive BCIs:** The outputs are derived from arbitrary brain activity which arises without the purpose of voluntarily controlling an application. The output signals contain implicit information about the user's mental state.

In common BCI applications, the user actively or indirectly controls an output device by changes of the brain signals according to a certain task (active and reactive BCIs). Active and reactive BCIs are mostly used to improve communication and environmental control for physically handicapped people, such as people with amyotrophic lateral sclerosis (ALS) or spinal cord injury (SCI) [16], [17]. With the utilization of passive BCIs (pBCIs), new applications emerge which can also be beneficial for healthy users. A pBCI was used in this thesis for cognitive state monitoring and will be described in more detail.

Utilization of pBCIs

In contrast to active and reactive BCIs, pBCIs are not used to voluntarily control an application, but to make use of implicit information of the brain signals [18]. Recently, pBCI systems have been used for monitoring the user's cognitive and mental state and enhancing the human-computer interaction with this implicit information [15], [19]. These pBCIs can be applied for mental state monitoring in combination with driving [13], [20],

[21] or teaching assistance [22], as well as adapting features of BCI systems according to the mental state changes [23], [24].

1.1.2 Brain Signals used for BCIs

BCI systems use various measurement modalities for the acquisition of brain signals, including both invasive and non-invasive techniques [25]. For invasive techniques, such as electrocorticography (ECoG) or single-cell recordings, the electrodes are placed on the surface of the cortex or even within the cortical tissue [26]. Non-invasive techniques on the other hand, such as EEG or functional near-infrared spectroscopy (fNIRS), use surface electrodes to record brain signals which are placed on the surface of the head (scalp) [27], [28]. Further non-invasive brain signal acquisition techniques are functional magnetic resonance imaging (fMRI) and magnetoencephalography (MEG). Due to the high costs and their constraint in mobility, fMRI and MEG systems are more commonly used in the field of basic brain research than for BCI applications [29]. For this thesis, the EEG was used as brain signal acquisition method and will therefore be explained in more detail.

Basic Principles of the EEG

The EEG basically measures electrical brain activity in form of potential differences caused by excitations of pyramidal nerve cells (Figure 1.2). An excitation of a nerve cell (neuron) yields a nerve impulse (action potential) which propagates from the cell body (soma) along the axon to the axon terminals. At the axon terminals, neurotransmitters are sent through synapses to the dendrites of another neuron. The neurotransmitters cause changes in the membrane potential of the post-synaptic neuron, so called post-synaptic potentials (PSPs). The PSPs create dipoles between the soma and apical dendrites of the neuron. The summation of the PSPs of many pyramidal neurons leads to potential differences, which can be measured with electrodes on the surface of the head (scalp) [30]–[33].

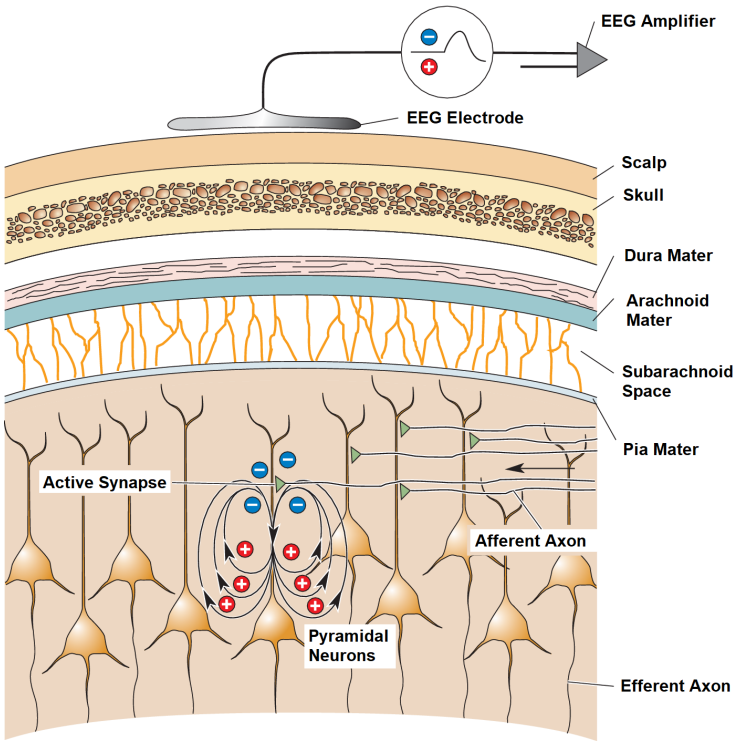

Figure 1.2: Physiological principle of the EEG: Potential differences generated by excitations of aligned pyramidal neurons (adapted from Bear et al. [32]).

EEG-based BCIs are also categorized according to the two types of brain signals: Event-related potentials (ERPs) and brain oscillations.

Event-related potentials (ERPs): An ERP can be seen as a measured brain response which is time- and phase-locked (evoked) to an external stimulus [34], [35]:

- **Evoked potentials (EPs):** An EP is the response of the brain to a sensory stimulus. The stimulus can be of auditory (AEP), visual (VEP) or somatosensory (SEP) origin [36], [37].
- **Steady-state EPs (SSEPs):** SSEPs can be elicited by a long, periodic presentation of a stimulus at a certain frequency. The frequency of the stimulation can be seen in the recorded EEG [38].

- **Slow cortical potentials (SCPs):** SCPs are slow negative or positive amplitude shifts in the EEG signal after a stimulus onset. Positive shifts are associated with movement, negative shifts with reduced cortical activity [29].

Brain Oscillations: Brain oscillations are also time-locked but not phase-locked (induced) responses, and can be the result of a change in the functional connectivity within neuronal networks [34]. Electrical brain activity consists of rhythmic components between 0.1 and 200 Hz.

Different mental states and functionalities can be distinguished based on brain activity at a certain frequency band (at a certain cortical area) [39]:

- **Delta band (0.5-4 Hz):** Deep sleep, trance and coma.
- **Theta band (4-8 Hz):** Deep relaxation, meditation and inhibition of responses [40].
- **Mu band (8-12 Hz):** Rest-state motor neurons (sensorimotor cortex) [41].
- **Alpha band (8-13 Hz):** Relaxation, closed eyes and inhibition of control.
- **Beta band (13-30 Hz):** Focused attention, high alert and active movement control (motor cortex).
- **Gamma band (>30 Hz):** High cognitive processes and cross-modal sensory processing (interactions between two or more different sensory modalities, such as vision and hearing) [42], [43].

Increased or decreased activity in a cortical area at a certain frequency band is known as event-related desynchronization or synchronization (ERD/ERS) [34], [44]:

- **Event-related desynchronization (ERD):** Decrease of synchrony within a neural network (only small groups of neurons work in synchrony), amplitude (power) decrease of a rhythmic component, activated cortical area and increased excitability.
- **Event-related synchronization (ERS):** Increase of synchrony within a neural network (many neurons work in synchrony), amplitude (power) increase of a rhythmic component, deactivated cortical area and decreased excitability.

Brain oscillation patterns in certain frequency bands can be used as indicators for mental state changes [45]–[47]. The following chapter describes the effects of mental state changes on brain signals and how to categorize them.

1.2 Introducing MWL and MF

Mental state changes, more precisely increasing MWL and MF, have effects on the electrophysiological signals (such as brain signals) and the performance of a person while executing a cognitive demanding task. MWL and MF are two important features for the usage of pBCIs, in the form of mental state monitoring systems [48].

1.2.1 Definition of MWL

Mental workload (MWL) can be defined as the number of tasks to be performed simultaneously, the load in working memory, or more generally as a measure of the quantity of mental resources engaged in a task [49], [50]. Therefore, MWL can be seen as a measure of task difficulty, and depends on each individual's capabilities and effort [51]. High MWL may affect people who use technology in their every day's life, such as interacting with computers, smartphones and other devices. Mental overload, as a result of high MWL, can compromise a user's performance and even safety by increasing error rates and reaction times [52], [53], and can lead to the neglection of critical information, known as cognitive tunneling [54]–[56].

1.2.2 Definition of MF

MF can be described as the feeling that may result from prolonged periods of cognitive activity. It is associated with exhaustion or tiredness, and can lead to a decrease in task performance and commitment [57], [58]. High MF may lead to the inability of a user to complete a task that requires self-motivation, without signs of cognitive failure or motor weakness [59].

It has been shown, that reduced motivation of a user to perform a task which induces high MF, is associated with increased sympathetic activity and decreased parasympathetic activity [60]–[62].

1.2.3 Methods for MWL and MF Detection

The methods of detecting MWL and MF can be divided into three main categories: Self-reporting and subjective ratings, behavioural measures and physiological measures [63].

Self-Reporting and Subjective Ratings

The subjective level of workload of participants can be determined with the NASA Task Load Index (TLX) questionnaire [64], the subjective level of fatigue with the Visual Analogue Scale to Evaluate Fatigue Severity (VAS-F) questionnaire [65]. Studies of Käthner et al. [48] and Roy et al. [49] have shown that if there is an increase in MWL and MF, there will be an increase of the subjective levels of workload and fatigue of the participants.

Behavioural Measures

Another method is to measure primary- and secondary-task performance, such as accuracy and reaction time [66]. If there is an increase in MWL and MF, there will be a decrease in the task performance (decrease of the accuracy and an increase of the reaction time) of the participants [48], [49]. Accuracy and reaction time of the participants can be recorded during the experiment and evaluated afterwards.

Physiological Measures

MWL and MF can be detected using the heart rate variability, oculomotor activity (eye movements), pupillometry (measure of pupil size and reflexes), electromyography (electrical activity produced by skeletal muscles), galvanic

skin responses (changes in sweat gland activity) and brain activity [67]. The physiological measure for MWL and MF detection used in this thesis is brain activity, more precisely amplitude power changes in certain frequency bands of the EEG signal. These changes are referred to as band power (BP) changes in the following.

1.3 State-of-the-Art pBCI Systems for Mental State Monitoring

Recently, more and more studies have emerged in the field of mental state monitoring in combination with pBCI systems. Lotte et al. [68] presented in 2019 state-of-the-art concepts which show that pBCI systems can be used for both online and offline applications. Offline systems are mainly used to evaluate the impact of products, performance, work settings or tasks on the user's mental state. Online applications however allow the system not only to detect, but also to be adapted based on the measured user's mental state [68]. In order to simulate real-life situations of the impact of the user's mental state on the task performance, virtual reality (VR) environments are more frequently used in combination with pBCI systems [69], [70].

Due to their portability and relatively low cost, most of the currently used pBCI systems are EEG-based [71]. Babiloni et al. presented in their study, that the implementation of BP features extracted from the EEG has been established to successfully detect and distinguish between different mental states of the user, such as MWL and MF. They reported, that an increase in MWL leads to a BP increase in the theta frequency band at frontal cortical areas with a simultaneous BP decrease in the alpha band at parietal areas [71]. These results corroborate the findings in the studies from Holm et al. [45], Stipacek et al. [46] and Scerbo et al. [47].

Klimesch et al. reported in their study [72], that increasing MF is associated with a BP increase in low frequency bands ($<$12 Hz) and a BP decrease in higher frequency bands ($>$12 Hz). The same observations were found in the study from Boksem et al. [57]. In another study, Käthner et al. [48] found

increasing alpha BP at parietal cortical areas and an increase in the theta BP, which represented an increase of MF.

The majority of pBCI systems uses classification algorithms based on the extracted EEG features to detect the different mental states of the user. Commonly used classifiers are for example the linear discriminant analysis (LDA) classifier and its variants (shrinkage or stepwise LDA), support vector machines (SVM) or k-nearest neighbours [68], [73]. Another classification approach is the so-called ensemble learning. The idea of this concept is to combine the use of different classifiers such as LDA, SVM and artificial neural networks (ANNs) [74] or use multiple base classifiers in a convolutional neural network (CNN) [75]. In order to improve classification accuracies, spatial filtering techniques like the common spatial pattern (CSP) algorithm are used in combination with a linear classifier, such as LDA [76]. The CSP algorithm maximizes the class separability by calculating the eigenvalues of the covariance matrix of the classes. Another concept which makes use of the eigenvalues of covariance matrices is the Riemannian geometry. Like presented from Yger et al. and Appriou et al., the Riemannian geometry can be used for feature representation and learning, classifier design and calibration time reduction [77], [78].

1.4 Aim of the Thesis and Hypothesis

The aim of this thesis was to detect high MWL and MF of participants performing a cognitive demanding task, based on their brain signals. Therefore, the letter n-back task [79] was used to mentally challenge and tire the participants. The brain signals were acquired non-invasively, using the EEG as signal imaging method. For MWL and MF detection, theta and alpha band power were used for subsequent signal processing and data analysis methods. The findings of the signal analysis were supported by self-reporting and subjective ratings, as well as behavioural measures of the participants. The Riemannian geometry was applied to the detection algorithm of high MWL and MF. As mentioned in Chapter 1.3, Riemannian geometry has already been used for classification algorithms. The novel approach for this thesis was to directly apply the Riemannian geometry on

the band power features of the EEG, to detect high increases in the theta and alpha frequency bands.

Based on the literature of state-of-the-art pBCI systems for mental state monitoring (Chapter 1.3), the following hypotheses can be derived: MWL and MF are reflected in BP changes of the EEG. An increase in theta BP and a decrease in alpha BP is expected during high MWL, whereas an increase in alpha BP is expected during high MF. The outcome of this thesis may be applied for further pBCI applications, where mental state changes play an important role. Such applications are for example a driving assistant or learning assistance system (a so-called Neurotutor).

2 Methods

This chapter describes the procedure of the experiment to record the brain signals from the participants while performing a demanding cognitive task. Furthermore, the signal processing, data and statistical analysis and data classification methods of the brain signals are described, as well as the algorithms for detecting high MWL and MF.

2.1 Experimental Procedure

The experimental design is illustrated in Figure 2.1. At the beginning and at the end of the experiment, a paradigm to intentionally record eye artefacts was presented, followed by the VAS-F questionnaire. In Run 0, the baseline EEG was recorded during a passive screening of the task (resting EEG). In run 1, 2 and 3, a paradigm was presented where the participants had to perform the letter n-back task [79]. After each task-run, the NASA-TLX questionnaire had to be filled in by the participants. The different parts of the experiment are described in more detail in the following sections.

The paradigms for the eye artefact recording, the passive screening and the letter n-back task were developed and presented using MATLAB® (Release 2019b, The MathWorks, Inc., Natick, Massachusetts, United States)[1] and the Psychtoolbox (Psychophysics Toolbox Version 3)[2]. The participants were seated on a desk chair in front of a monitor, where the paradigms were presented. A Keyboard was used by the participants to perform the letter n-back task.

[1] https://mathworks.com/
[2] http://psychtoolbox.org/

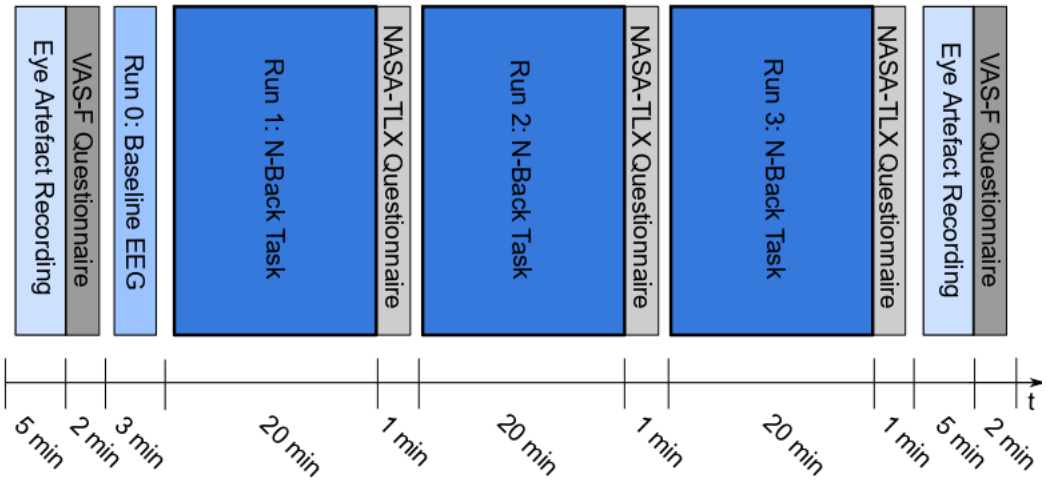

Figure 2.1: Experimental design: Paradigm for eye artefact recording at the beginning and at the end of the experiment, followed by the VAS-F questionnaire; Run 0: passive screening of the task to record the baseline EEG; Run 1, 2 and 3: performing letter n-back task, followed by NASA-TLX questionnaire.

2.1.1 Eye Artefact Recording

Artefacts due to eye movements, blinks and saccades strongly affect the EEG signal, and should therefore be corrected [80], [81]. At the beginning and at the end of the experiment, a paradigm to intentionally record these eye artefacts was presented. The paradigm used in this thesis for the recording, as well as the algorithms for detecting and correcting the eye artefacts were introduced by Kobler et al. [82]. The paradigm included four different conditions: rest, horizontal, vertical and blink.

1. **Rest:** A blue circle was presented on a black screen (Figure 2.4). The participants had to fixate the blue circle without moving or blinking.
2. **Horizontal:** The blue circle was moving between the left and right side of the screen. The participants had to follow the blue circle with their eyes.
3. **Vertical:** The participants had to follow the blue circle with their eyes moving up and down on the screen.

Figure 2.2: Paradigm for eye artefact correction: Condition rest (adapted from Kobler et al. [82]).

4. **Blink:** The blue circle was shrinking and enlarging at a certain frequency. The participants had to blink according to that frequency.

2.1.2 Recording Baseline EEG

In Run 0, a passive screening of the task was conducted. The participants were instructed to calmly look at the screen were the paradigm was presented, but without performing the task. In this way, the resting EEG of the participants was recorded, which was used as baseline EEG in the signal processing and data analysis part. The BP changes for detecting increasing MWL and MF were calculated with the differences between the baseline EEG and the task-run EEG. Detailed information about the calculation of the BP differences can be found in Chapter 2.4 (Signal Processing).

2.1.3 Performing N-Back Task

In run 1, 2 and 3, a paradigm was presented where the participants had to perform the letter n-back task with varying difficulty. The paradigm of the

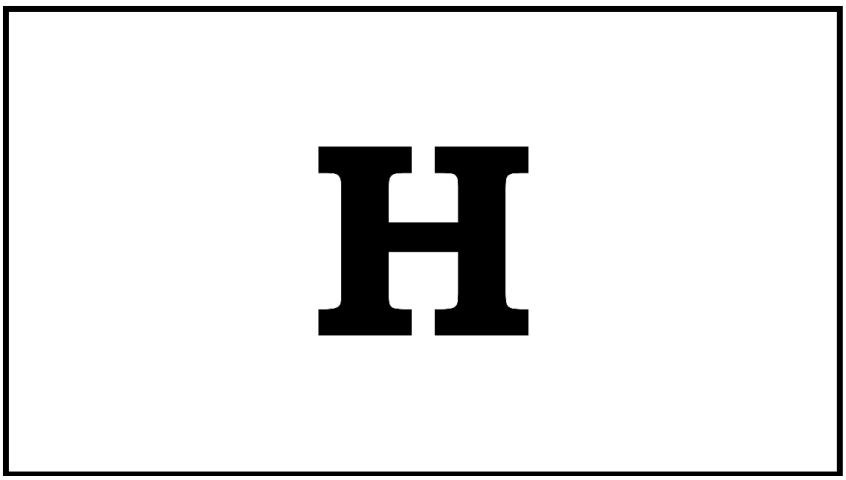

Figure 2.3: Presentation of a letter during the n-back task.

task was designed to exhaust and tire the participants, in order to elicit an increase in MWL and MF.

Letter N-Back Task

The letter n-back task consisted of a sequence of 20 letters. An example of the letter presentation is shown in Figure 2.3. The goal of the task was to identify target letters within the sequence. A target letter was defined as follows: If the currently presented letter is the same as n letters back, the current letter is a target letter. In each sequence, five target letters were included. In order to avoid creating short words, which would facilitate the task, only consonants were used. During the experiment, three different n-back tasks were presented: 1-back, 2-back and 3-back.

Paradigm and Trial Structure

The trial structure of the task runs can be seen in Figure 2.4. At the beginning of the trial, the instruction of the current task was presented for 2 seconds, in order to inform the participants which n-back task they had to perform. In the reference phase, a fixation cross was shown, again for 2 seconds. The

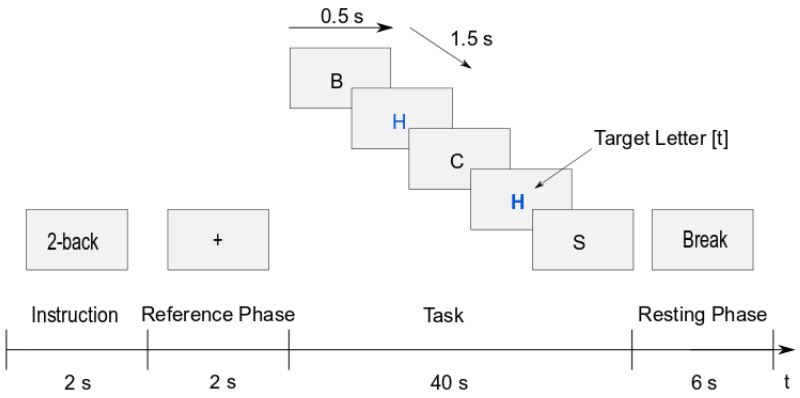

Figure 2.4: Trial structure of the letter n-back task (example 2-back): Instruction (2 s), reference phase (2 s), task (40 s) and resting phase (6 s).

task itself had a duration of 40 seconds. Each letter was presented for 0.5 seconds, with 1.5 seconds pause between the letters. During the pause, the fixation cross was shown again, in order to avoid random eye movements of the participants. If a target letter was identified, the participants had to press the *t* key. After the task, there was a 6 seconds break, before the next trial started.

Each of the three conditions of the task-run (1-back, 2-back and 3-back) was presented eight times, which led to 24 trials per run. One trial lasted for 50 seconds, resulting in a total duration of 20 minutes per run.

2.1.4 VAS-F and NASA-TLX Questionnaires

The questionnaires were used to support the findings in the brain signals. Their results should help to evaluate, if the experiment was demanding enough to elicit high MWL and MF of the participants.

The VAS-F questionnaire had to be filled in by the participants at the beginning and at the end of the experiment, after the eye artefact correction paradigm. This questionnaire evaluated the self-reporting and subjective

rating of MF in the participants and consisted of 18 questions concerning individual levels of fatigue and energy (ratings from 0 to 10).

The NASA-TLX questionnaire had to be filled in by the participants after each task-run, in order to evaluate the self-reporting and subjective rating of MWL. This questionnaire consisted of six questions concerning workload (ratings from 0 to 20).

2.2 Participants

20 healthy participants were measured (7 female and 13 male). The participants had normal or corrected to normal vision. Their age ranged from 21 to 31 years, with a mean of 26.15 years and a standard deviation of 2.6 years. Before the experiment, the participants got all necessary information about the procedure of the experiment and voluntarily gave their written informed consent. They were instructed to sit calmly on their chair and avoid (as good as possible) eye, head and body movements during the experiment.

2.3 Signal Acquisition

This section describes the amplifier, recording software, electrode setup and further applications used for acquiring the EEG signals.

2.3.1 Electrode Setup

The amplifier used for the recording and amplification of the brain signals and the eye artefacts was the BrainVision LiveAmp (Brain Products GmbH, Gilching, Germany). The LiveAmp is a compact wireless EEG amplifier, especially designed for mobile EEG applications[3]. The amplifier was connected to the electrodes and placed in a pocket of the cap on the back of the participant's head. The amplified signals were preprocessed (50 Hz

[3]https://www.brainproducts.com/

notch filter) and sent via blue tooth connection to a personal computer (PC). As a recording software, the BrainVision Recorder (Brain Products GmbH, Gilching, Germany) was used. The brain signals and the eye artefacts were recorded at a sampling rate of 500 Hz.

For the acquisition of the brain signals and the eye artefacts, 32 active electrodes were used. The layout of the electrodes was modified from the Standard 32Ch actiCAP snap for LiveAmp (Easycap GmbH, Herrsching, Germany) and can be seen in Figure 2.5. To acquire the EEG signals, 28 electrodes were used at the following positions: Fp1, Fp2, F7, F3, Fz, F4, F8, FC5, FC1, FC2, FC6, T7, C3, Cz, C4, T8, CP5, CP1, CP2, CP6, P7, P3, Pz, P4, P8, O1, Oz and O2. Three electrodes were used for the electrooculography (EOG), in order to record the eye artefacts. The electrodes were fixed with adhesive rings on the forehead (EOGM), on the left (EOGL) and on the right cheek (EOGR) of the participants. The ground electrode (GND) was placed at position Fpz, the reference electrode (REF) at position FCz. The electrode used for optional re-referencing (RE-REF) was mounted at the right mastoid of the participants.

2.4 Signal Processing

This chapter describes the signal processing chain from the raw EEG and EOG signals to the clean EEG signal. The individual steps of the signal processing chain are illustrated in Figure 2.6 and can be divided into three blocks: preprocessing, eye artefact correction (adapted from Kobler et al. [82]) and muscle artefact correction. The signal processing was implemented in MATLAB®, supported with adapted functions from the EEGLAB toolbox[4] [83].

In addition to the brain signals and the eye artefacts, the paradigm markers had to be recorded. The paradigm markers are necessary for the analysis of the EEG signals, in order to find the exact positions in the EEG signal of specific trial states (instruction, reference phase, task or resting phase), as well as to identify the task condition (1-back, 2-back or 3-back) in a trial. The

[4] http://www.sccn.ucsd.edu/eeglab/

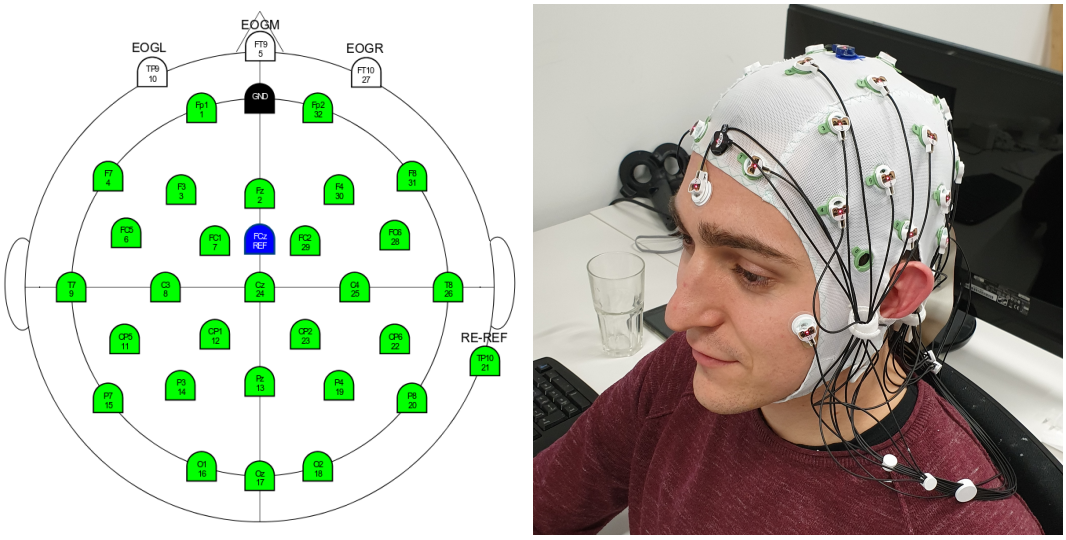

(a) Modified electrode layout with positions and labels

(b) Electrode montage on the participant's head

Figure 2.5: Electrode setup with 32 electrodes: 28 EEG electrodes (green), 3 EOG electrodes (white: EOGL, EOGM, EOGR), 1 electrode for optional re-referencing (green: RE-REF) and ground (black: GND) and reference (blue: REF) electrode.

paradigm markers were generated with MATLAB® during the presentation of the paradigm. To guarantee an accurate timing, the markers must be recorded time-synchronized with the EEG and the EOG signals. Therefore, the signals and the markers were linked via lab streaming layer (LSL) [84] and recorded with the LabRecorder (default recording program for LSL)[5]. With the LabRecorder, the recorded signals were saved to an extensible data format (XDF) file.

2.4.1 Preprocessing

The first signal processing step was a 50 Hz notch filter, which was applied during the recording of the signals. A notch filter is a band-stop filter with a narrow stop band (high quality (Q) factor) and is usually applied to remove the 50 Hz power line interference [85].

[5]https://github.com/sccn/lsl_archived/wiki/LabRecorder.wiki/

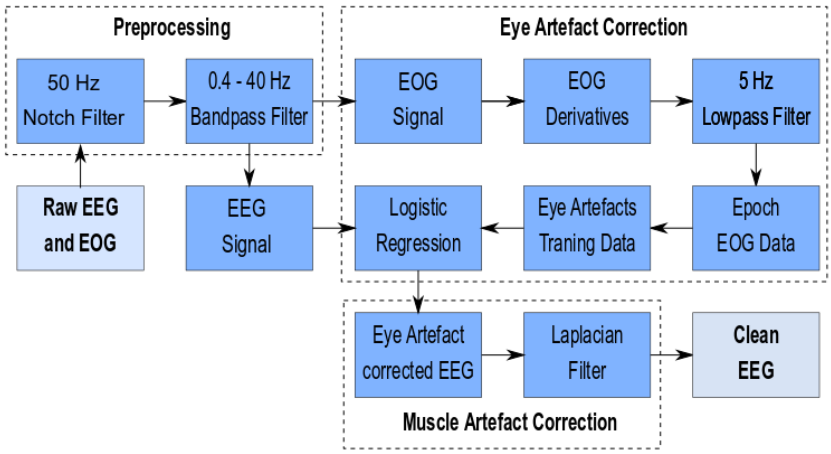

Figure 2.6: Signal processing chain: The individual steps from the raw EEG and EOG signal to the clean EEG signal can be divided into three blocks. Preprocessing, eye artefact correction (adapted from Kobler et al. [82]) and muscle artefact correction.

The next step was to bandpass-filter the EEG and EOG signals between 0.4 and 40 Hz. In that way, the unwanted direct current component (0 Hz), the low (< 0.4 Hz) and the high (> 40 Hz) frequency components were removed. The used filter was a 4^{th}-order Butterworth filter and implemented with the MATLAB® function `filtfilt` (zero-phase bi-directional filter).

2.4.2 Eye Artefact Correction

The eye artefact correction block was adapted from Kobler et al. [82]. The first step was to calculate the EOG derivatives from the three EOG electrodes (EOGL, EOGM, EOGR):

1. **Horizontal EOG derivate (HEOG):** The difference between left and right eye movements was calculated with Equation 2.1:

$$HEOG = EOGR - EOGL \tag{2.1}$$

2. **Vertical EOG derivate (VEOG):** The VEOG describes the average of

the left eye and the right eye movements (Equation 2.2):

$$VEOG = \frac{EOGM - EOGR}{2} + \frac{EOGM - EOGL}{2} \tag{2.2}$$

3. **Radial EOG derivate (REOG):** The calculation of average of the movements in all EOG channels can be seen in Equation 2.3:

$$REOG = \frac{EOGM + EOGR + EOGL}{3} \tag{2.3}$$

Next, a lowpass filter was applied on the EOG derivatives, in order to remove the unwanted higher frequency components. The used filter was a 2^{nd}-order Butterworth filter with a cutoff frequency of 5 Hz, also implemented with the MATLAB® function `filtfilt`. The lowpass-filtered EOG derivatives were divided into trials (epochs). Therefore, the EOG paradigm markers were used to cut the continuous signal into epochs of the same length, as well as to distinguish between the four conditions (rest, horizontal, vertical and blink). Noisy trials were then excluded after visual inspection.

With the information about the eye movements from the eye artefact paradigm and the EOG derivative epochs, a training data set could be generated. The training data was fitted into the eye artefact correction algorithm and consisted of six different artefact classes: right, left, up, down, blink and rest. The algorithm used a penalized logistic regression model to classify the eye artefacts and remove them from the EEG signal. Detailed information about the eye artefact correction can found at [82].

2.4.3 Muscle Artefact Correction

Besides artefacts from eye movements and blinks, the EEG signal can also be contaminated with artefacts from muscle contractions. Spatial filtering in form of the Laplacian filter has been proven to be an effective method to remove these muscle artefacts [86].

Equation 2.4 shows an example of the application of the Laplacian filter: the signal at a certain electrode (Cz) is subtracted by the mean of its four surrounding electrodes (FC1, FC2, CP1, CP2).

$$Cz_{Lap} = Cz - \frac{FC1 + FC2 + CP1 + CP2}{4} \tag{2.4}$$

In order to find the four nearest neighbours of each electrode, an electrode location file was used. The location file was provided by Easycap and adapted to the electrode layout used in the experiments.

2.5 Data Analysis

After the preprocessing and artefact correction of the signals (Chapter 2.4), the cleaned EEG signal could be used for further data analysis. This section describes the steps to get from the cleaned EEG signal to the band power (BP) differences between the EEG from the task-runs and the baseline EEG in different frequency bands. Furthermore, the methods to conduct the statistical analyses and the classification of the dataset are described, as well as the algorithms to define and detect high MWL and MF.

2.5.1 Calculating BP Differences

The first step was to generate the different frequency bands for the BP differences. The frequency bands were generated by applying a 4^{th}-order Butterworth bandpass filter, again by using the MATLAB® function `filtfilt`. The desired frequency bands were the theta (4-8 Hz) and the alpha band (8-13 Hz).

After the EEG signals were divided into different frequency bands, the continuous signals were divided into single trial signals (epochs) and separated by the three task conditions (1-back, 2-back and 3-back). The calculation of the band power (BP) of a single trial can be seen in Equation 2.5:

$$BP = \log_{10}\left(\sum_{n=1}^{N} signal(n)^2\right) \tag{2.5}$$

The *signal* used for the calculation of the BP, was the Fourier-transformed EEG signal during the task phase (40 s) of a single trial. For the Fourier transform, the MATLAB® function `fft` was used (fast Fourier transform, single-sided). Each time-point of the *signal* was squared and summed up over the whole task phase. The decadic logarithm was used to scale the results of the amplitude power.

The BP calculation according to Equation 2.5 was performed for the task-run EEG in both frequency bands (theta and alpha), for each trial in each condition (1-back, 2-back and 3-back). In order to get the BP changes after each single trial of the experiment, each BP result from the task-run EEG was subtracted by the mean of the baseline EEG (averaged over all three trials). The mean of the baseline EEG was used to compare BP results from signals of equal length.

For the grand average analysis, the participants were divided into two groups according to their task performance: Group 1 (high performers) and Group 2 (low performers). The segmentation was done by the median split of the task performance of the participants.

2.5.2 Statistical Analyses

For the statistical analyses, the BP changes of each condition (1-back, 2-back and 3-back) for each run (run 1, run 2 and run 3) were inspected. The BP changes of the individual trials were averaged over a whole run, for each condition separately. Furthermore, the individual channels were summed up to four regions of interest (ROIs):

1. **Frontal:** Fp1, Fp2, F7, F3, Fz, F4 and F8.
2. **Central:** FC5, FC1, FC2, FC6, C3, Cz and C4.
3. **Parietal:** CP5, CP1, CP2, CP6, P7, P3, Pz, P4 and P8.
4. **Occipital:** O1, Oz and O2.

Again, the participants were divided into two groups, according to their task performance (see Chapter 2.5.1). The statistical analyses were conducted for both frequency bands (theta and alpha) separately. With the aforementioned parameters, a 3x3x4 repeated measures analysis of variance (ANOVA) was

conducted. The within factors included the runs (run 1, 2 and 3), the conditions (1-back, 2-back and 3-back) and the ROIs (frontal, central, parietal and occipital). The between factors were generated from the two participant groups.

For further investigations of the parameters and their influence on the BP changes, a post hoc analysis was conducted. With this analysis, the BP changes from each run, condition and ROI were compared, as well as the influence of the two participant groups (high and low performers). Both the repeated measures of ANOVA and the post hoc analyses were performed with the free and open statistical software Jamovi[6].

2.5.3 Detection of high MWL and MF

For the detection of high MWL and MF, the Riemannian geometry approach was implemented. Riemannian geometry has already been introduced to detect artefacts in an EEG signal, by calculating the Riemannian distance of a signal to a defined threshold of the reference (baseline) signal [87].

Calculating Threshold with Baseline EEG

As a first step, the covariance matrix of the reference signal (baseline EEG) was calculated:

$$C_{ref} = \frac{1}{N_{ref} - 1} \cdot X_{ref} X_{ref}^{T} \tag{2.6}$$

In Equation 2.6, the covariance matrix ($X_{ref} X_{ref}^{T}$) is scaled by the number of samples N_{ref} of the reference signal.

After that, a window of 500 samples and a step size of 125 samples were defined to step through the reference signal. For the window, the covariance matrix C_{win} was calculated by using Equation 2.6. The combined eigenvalues

[6] https://www.jamovi.org/

of the covariance matrices of the window C_{win} and the reference signal C_{ref} were calculated with Equation 2.7:

$$\lambda = eig\left(C_{win}^{-1/2} C_{ref} C_{win}^{-1/2}\right) \tag{2.7}$$

The eigenvalues λ were then generated by using the MATLAB® function `eig`. The distance of the window to the reference signal was calculated by summing up the logarithmic power of each eigenvalue and taking its square root [88]:

$$D_R = \sqrt{\sum_{n=1}^{N} log_{10}(\lambda_n)^2} \tag{2.8}$$

With Equation 2.8, the distance D_R of the window to the reference signal was calculated for each step through the reference signal. The threshold of the reference signal $THRS$ resulted from Equation 2.9:

$$THRS = mean(D_R) + 2.5 \cdot std(D_R) \tag{2.9}$$

Calculating Riemannian Distances with Task-Run EEG

For calculating the distances of the task-run EEG, the same procedure as for calculating the Riemannian distances for threshold was applied. For that, the distance for each condition in each run for both frequency bands (theta and alpha) was calculated. Again, a window of 500 samples and a step size of 125 samples were defined. For each step, the covariance matrix of the window and its eigenvalues λ were calculated by using Equations 2.6 and 2.7. As C_{ref}, the covariance matrix of the reference signal (baseline EEG) was used. The Riemannian distances D_R of the eigenvalues were again computed with Equation 2.8.

In order to detect high MWL and MF, the Riemannian distances of each step through the task signal (task-run EEG) were averaged over trials and task conditions, and compared with the threshold of the reference signal $THRS$

(baseline EEG). If the average of the Riemannian distance D_R reached or surpassed the threshold, high MWL and MF were detected in the participants. The distances were calculated for both frequency bands (theta and alpha).

3 Results

3.1 Grand Average BP Changes

In order to obtain the BP changes over time, a grand average analysis (average over all participants) was conducted for the theta and the alpha frequency band separately. The BP changes of each trial were averaged over the task conditions (1-back, 2-back and 3-back) at each run. Additionally, the BP changes for each frequency band were divided into a high and a low performance group (PG).

The BP changes of the theta frequency band of the high performers are illustrated in Figure 3.1, the BP changes of the low performers in Figure 3.2. For both PGs, there is a slight BP increase in run 1 and run 2. For the high performers however, the BP slightly decreases again in run 3, whereas the low performers show a high BP increase. The most significant differences between high and low performers were found at the 1-back task in run 3. The BP changes for both PGs are most prominent at the parietal cortex.

The grand average results of the BP changes in the alpha frequency band show a slightly different behaviour for both the high (Figure 3.3) and the low performers (Figure 3.4). For both PGs, there is a BP decrease in run 1, followed by a slight BP increase in run 2. Like the findings in the theta band, the BP of the high performers slightly decreases again in run 3, whereas the BP of the low performers shows a high increase. Again, the most significant differences between high and low performers were found at the 1-back task in run 3. In Contrast to the theta band, the BP changes for both PGs in the alpha band are most prominent at the central cortex.

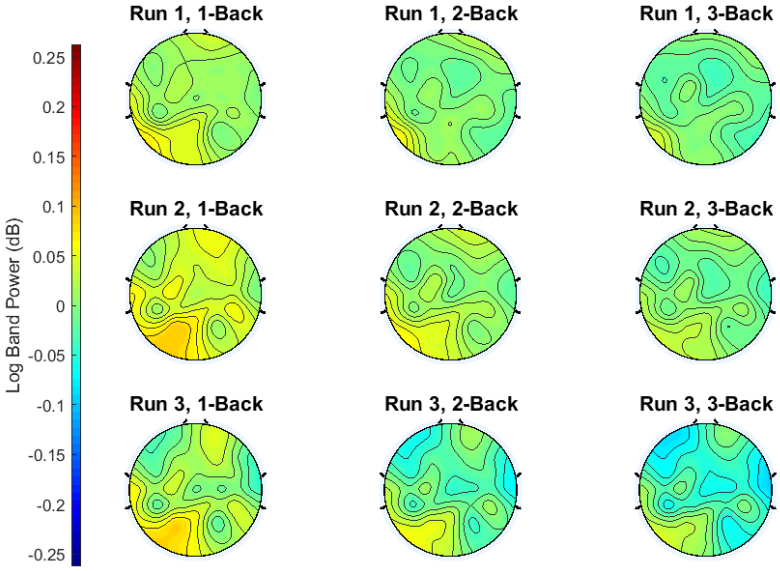

Figure 3.1: Grand average theta BP changes of the high PG. The task conditions are averaged over all trials at each run.

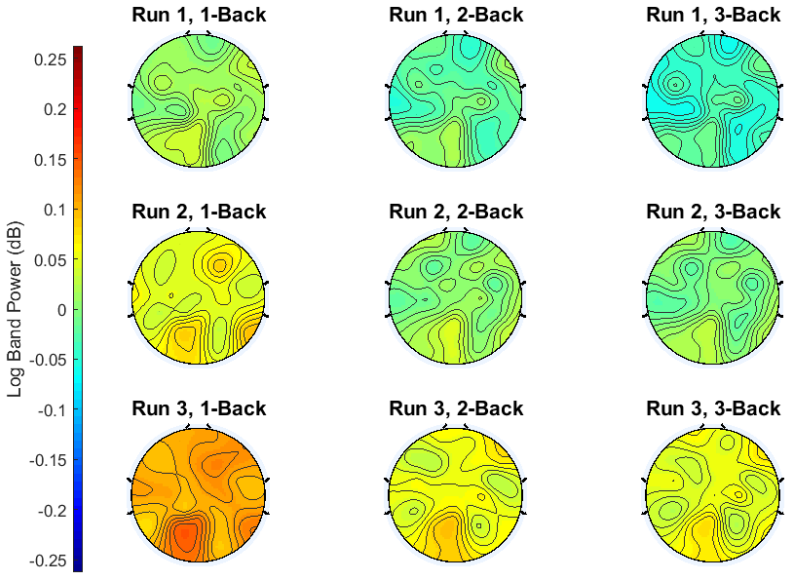

Figure 3.2: Grand average theta BP changes of the low PG. The task conditions are averaged over all trials at each run.

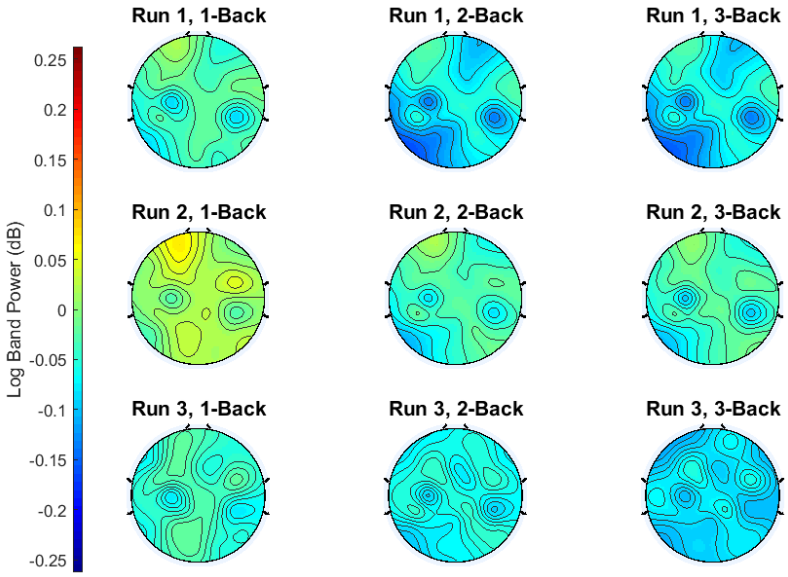

Figure 3.3: Grand average alpha BP changes of the high PG. The task conditions are averaged over all trials at each run.

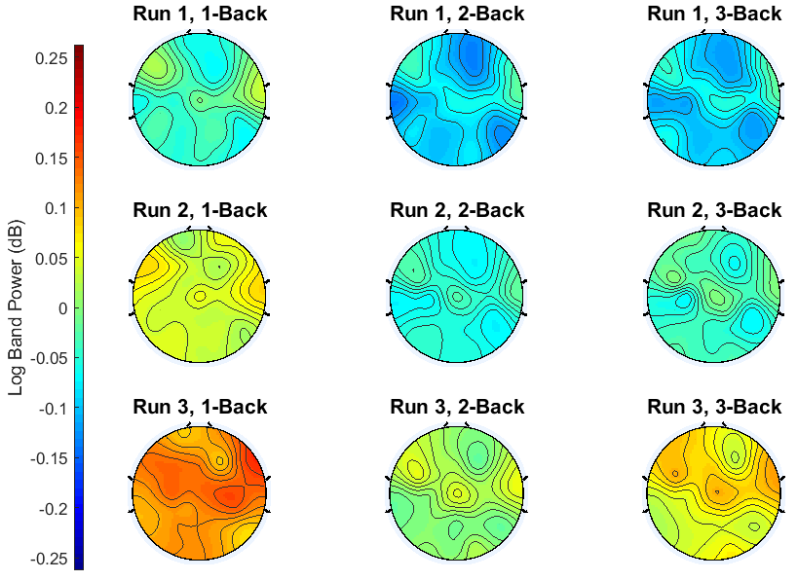

Figure 3.4: Grand average alpha BP changes of the low PG. The task conditions are averaged over all trials at each run.

3.1.1 Statistical Analyses

For further investigations of the BP changes, the estimated marginal means for both frequency bands (theta and alpha) were computed. For that, the mean and the standard error (SE) of the BP changes were calculated for each PG (high and low), task (1-back, 2-back and 3-back) and ROI (frontal, central, parietal and occipital) at each run.

Figure 3.5 shows the mean and the SE of the high (orange line) and the low (blue line) PG of each run at the theta (a) and the alpha (b) frequency band. For both frequency bands, the low PG shows a higher BP increase than the high PG. The differences are most prominent at run 3, where the BP increase of the high performers goes into saturation, while the BP of the low performers keeps increasing.

The mean and the SE of the individual tasks at each run are illustrated in Figure 3.6. For both the theta (a) and the alpha (b) frequency band, the 1-back task (blue line) and the 2-back task (gray line) show the same behaviour: A high BP increase from run 1 to run 2, followed by a lower increase from run 2 to run 3. The BP differences of the 1-back task however are significantly higher than for the 2-back task. At the theta band, the 3-back task (orange line) has the lowest BP difference at each run, but the highest BP increase from run 2 to run 3. The BP differences at the alpha band of the 3-back task are very similar to the 2-back task at run 1 and run 2. From run 2 to run 3 however, the BP increase of the 3-back task is higher than the increase of the 1-back and 2-back task, similar to the behaviour at the theta band.

In Figure 3.7 the mean and the SE of the BP changes of the individual ROIs (frontal, central, parietal and occipital) at each run are displayed. The results of the theta frequency band (a) differ from the results of the alpha frequency band (b): The BP at the theta band increases continuously at each ROI, while the BP at the alpha band increases higher from run 1 to 2 than from run 2 to 3. Furthermore, at the theta band, the central (gray line) and the parietal cortex (orange line) contain the highest BP differences between the baseline and the task-runs, whereas the highest BP differences at the alpha band are found at the frontal (blue line) and the occipital cortex (green line).

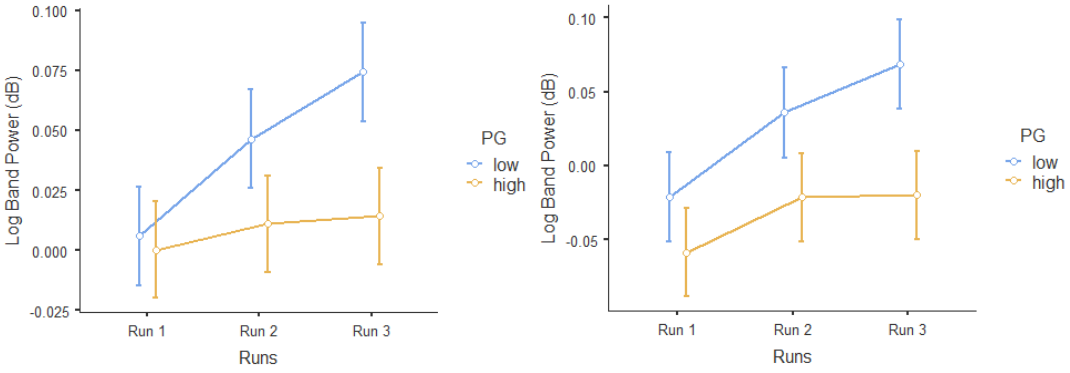

(a) Theta BP changes

(b) Alpha BP changes

Figure 3.5: Theta (a) and alpha (b) BP changes of the high and low PG at each run.

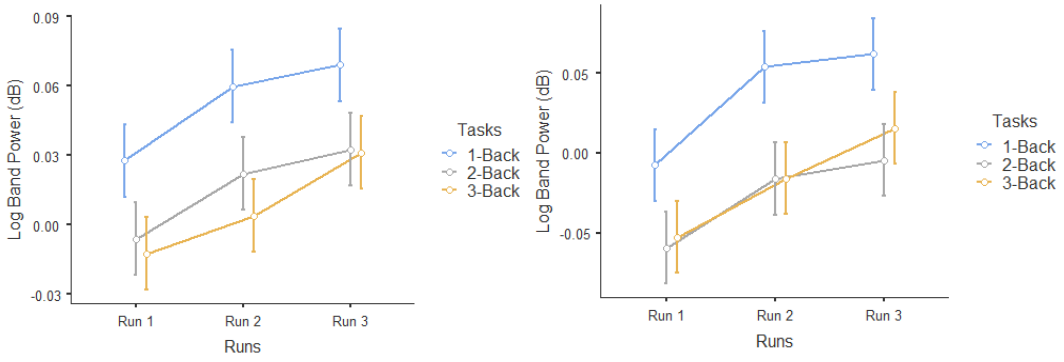

(a) Theta BP changes

(b) Alpha BP changes

Figure 3.6: Theta (a) and alpha (b) BP changes of the task conditions at each run.

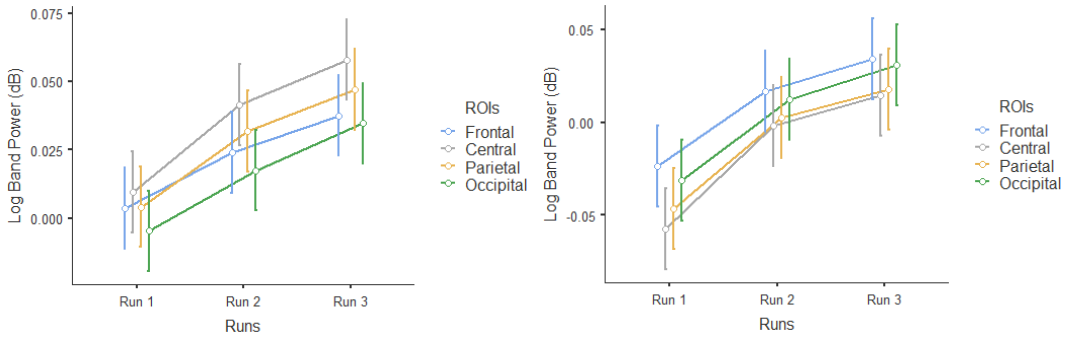

(a) Theta BP changes

(b) Alpha BP changes

Figure 3.7: Theta (a) and alpha (b) BP changes of the individual ROIs at each run.

In addition to the estimated marginal means, the statistical analyses included a 3x3x4 repeated measures ANOVA and several post-hoc tests. In Table 3.1, the within subjects effects of the 3x3x4 repeated measures ANOVA are presented for the theta and the alpha frequency bands, in Table 3.2 the between effects. As within factors the *Runs* (run 1, run 2 and run 3), the *Tasks* (1-back, 2-back and 3-back) and the *ROIs* (frontal, central, parietal and occipital) were used, as between factors the *PGs* (high and low). The tables include the degrees of freedom (df1 and df2), the F-values and the Greenhouse-Geisser corrected p-values. The significance level was defined as $\alpha = 0.01$. The factor *Runs* revealed no significance in the theta band ($F(2,36) = 6.23$, $p = 0.02$), but a significant main effect at the alpha band ($F(2,36) = 13.42$, $p < 0.01$). The factor *Tasks* reached statistical significance in both the theta ($F(2,36) = 16$, $p < 0.01$) and the alpha band ($F(2,36) = 23.04$, $p < 0.01$). For the factor *ROIs*, a significant main effect was reached in the theta band ($F(3,54) = 7.04$, $p < 0.01$), whereas the alpha band ($F(3,54) = 4.07$, $p = 0.04$)revealed no significance. The between subjects effects with the factor *PGs* did not reach significance in either of the frequency bands (theta: $p = 0.20$, alpha: $p = 0.15$).

Table 3.1: Within subjects effects of the 3x3x4 repeated measures ANOVA of the theta and the alpha frequency band.

Measure	Theta Band				Alpha Band			
	df1	df2	F	p_{GG}	df1	df2	F	p_{GG}
Runs	2	36	6.23	0.02	2	36	13.42	**<0.01**
Tasks	2	36	16	**<0.01**	2	36	23.04	**<0.01**
ROIs	3	54	7.04	**<0.01**	3	54	4.07	0.04
RunsxTasks	4	72	0.81	0.48	4	72	1.51	0.23
RunsxROIs	6	108	2.37	0.11	6	108	1.90	0.15
TasksxROIs	6	108	3.63	0.03	6	108	2.23	0.12
RunsxTasksxROIs	12	216	0.64	0.50	12	216	0.92	0.427

Table 3.2: Between subjects effects of the 3x3x4 repeated measures ANOVA of the theta and the alpha frequency band.

Measure	Theta Band				Alpha Band			
	df1	df2	F	p_{GG}	df1	df2	F	p_{GG}
PG	1	18	7.74	0.20	1	18	2.33	0.15

For the post-hoc tests, the PGs, the tasks and the ROIs were compared with each other at each run, using the Bonferroni method. The t-values (with its degree of freedom) and the Bonferroni corrected p-values were calculated for both frequency bands separately.

Table 3.3 shows the comparisons of the low and high PG. For the low performers, statistically significant difference was reached between run 1 and run 3 for both the theta band (t(19) = -3.91, $p < 0.01$) and the alpha band (t(19) = -4.72, $p < 0.01$). In the alpha band, the comparison between run 1 and run 2 also showed a low p-value, but the difference did not reach statistical significance (t(19) = -3.00, p = 0.07). For the low PG, the lowest p-values were found between run 1 and run 3 as well, but the comparisons did not reveal a statistically significant difference in neither the theta (t(19) = -0.89, p = 0.23) nor the alpha band (t(19) = -2.24, p = 0.47).

In Table 3.4, the comparisons of the task conditions are presented. In the alpha band, the comparisons reached statistically significant difference in the 1-back task between run 1 and run 2 (t(19) = -4.13, $p < 0.01$) and between run 1 and run 3 (t(19) = -4.66, $p < 0.01$), as well as in the 3-back task between run 1 and run 3 (t(19) = -4.57, $p < 0.01$). In the theta band, no statistically significant differences were revealed, but the comparisons with the lowest p-values were also found between run 1 and run 3 in the 1-back (t(19) = -3.03, p = 0.13) and the 3-back task (t(19) = -3.19, p = 0.08).

The comparisons of the individual ROIs are presented at Table 3.5. Statistically significant difference in the alpha band was found between run 1 and run 3 at each ROI: at the frontal (t(19) = -4.36, $p < 0.01$), the central (t(19) = -5.46, $p < 0.01$), the parietal (t(19) = -4.86, $p < 0.01$) and the occipital cortex (t(19) = -4.68, $p < 0.01$). Additionally, the comparison between run

1 and run 2 showed statistical significance at the central cortex (t(19) = -4.19, p < 0.01). In the theta band, no comparison reached a statistically significant difference, but the lowest p-values could be found at each ROI as well between run 1 and run 3, with the lowest at the central cortex (t(19) = -4.01, p = 0.02).

Table 3.3: Post-hoc test comparisons of the low and high PG at different runs.

Comparisons			Theta Band		Alpha Band	
			t(19)	p_{Bonf}	t(19)	p_{Bonf}
Low PG	Run 1	Run 2	-2.32	0.40	-3.00	0.07
	Run 1	Run 3	-3.91	< **0.01**	-4.72	< **0.01**
	Run 2	Run 3	-1.59	1.00	-1.72	1.00
High PG	Run 1	Run 2	-0.68	1.00	-2.16	0.56
	Run 1	Run 3	-0.89	0.23	-2.24	0.47
	Run 2	Run 3	-0.21	1.00	-0.08	1.00

Table 3.4: Post-hoc test comparisons of the 1-back, 2-back and 3-back task at different runs.

Comparisons			Theta Band		Alpha Band	
			t(19)	p_{Bonf}	t(19)	p_{Bonf}
1-Back	Run 1	Run 2	-2.35	0.79	-4.13	< **0.01**
	Run 1	Run 3	-3.03	0.13	-4.66	< **0.01**
	Run 2	Run 3	-0.68	1.00	-0.53	1.00
2-Back	Run 1	Run 2	-2.07	1.00	-2.90	0.19
	Run 1	Run 3	-2.83	0.23	-3.68	0.02
	Run 2	Run 3	-0.76	1.00	-0.78	1.00
3-Back	Run 1	Run 2	-1.20	1.00	-2.46	0.60
	Run 1	Run 3	-3.19	0.08	-4.57	< **0.01**
	Run 2	Run 3	-1.99	1.00	-2.11	1.00

Table 3.5: Post-hoc test comparisons of the individual ROIs at different runs.

Comparisons			Theta Band		Alpha Band	
			t(19)	p_{Bonf}	t(19)	p_{Bonf}
Frontal	Run 1	Run 2	-1.70	1.00	-3.03	0.28
	Run 1	Run 3	-2.82	0.50	-4.36	$<$ **0.01**
	Run 2	Run 3	-1.12	1.00	-1.34	1.00
Central	Run 1	Run 2	-2.64	0.78	-4.19	$<$ **0.01**
	Run 1	Run 3	-4.01	0.02	-5.46	$<$ **0.01**
	Run 2	Run 3	-1.37	1.00	-1.26	1.00
Parietal	Run 1	Run 2	-2.30	1.00	-3.71	0.04
	Run 1	Run 3	-3.56	0.07	-4.86	$<$ **0.01**
	Run 2	Run 3	-1.26	1.00	-1.15	1.00
Occipital	Run 1	Run 2	-1.84	1.00	-3.30	0.13
	Run 1	Run 3	-3.27	0.15	-4.68	$<$ **0.01**
	Run 2	Run 3	-1.43	1.00	-1.38	1.00

3.2 Subjective Ratings and Behavioural Measures

In addition to the BP changes of the EEG, subjective ratings and behavioural measures can be used to determine increasing MWL and MF. For the subjective ratings, VAS-F and NASA-TLX questionnaires were conducted before, during and after the experiments. As behavioural measures, the task performance accuracies and the response times were used.

3.2.1 Subjective Ratings

In Figure 3.8, the single subject and grand average ratings according to the VAS-F questionnaires are illustrated. The questionnaires were taken before (blue bars) and after the experiments (orange bars) and divided into two categories, the fatigue level (A) and the energy level (B). The highest possible score of both rating categories was scaled to 100%, in order to make them more comparable. For all subjects, the fatigue level increased during the experiment and the energy level decreased. The grand average rating of the fatigue level increased from 24% to 54%, the energy level decreased from 65% to 46%.

The single subject and grand average ratings of the NASA-TLX questionnaires are shown in Figure 3.9. The questionnaires were conducted after run 1 (blue bars), run 2 (orange bars) and run 3 (yellow bars). Again, the highest possible rating score was scaled to 100 %. The results of the individual subjects show a diverging behaviour: For some, the task load increased during the experiment, for others the task load stayed the same or even decreased. However, the grand average ratings of the task load increased continuously after each run (56%, 63% and 68%).

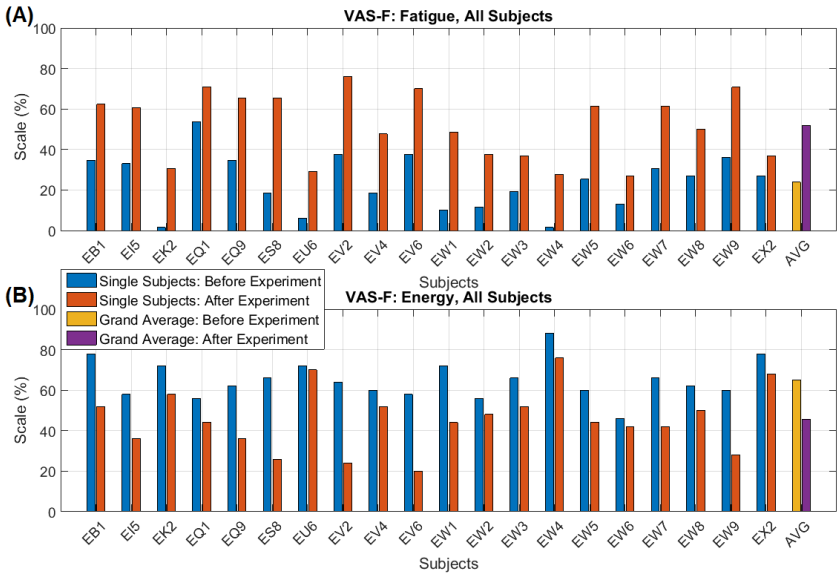

Figure 3.8: Single subject and grand average ratings according to the VAS-F questionnaires, before and after the experiment. (A): Fatigue level, (B): Energy level.

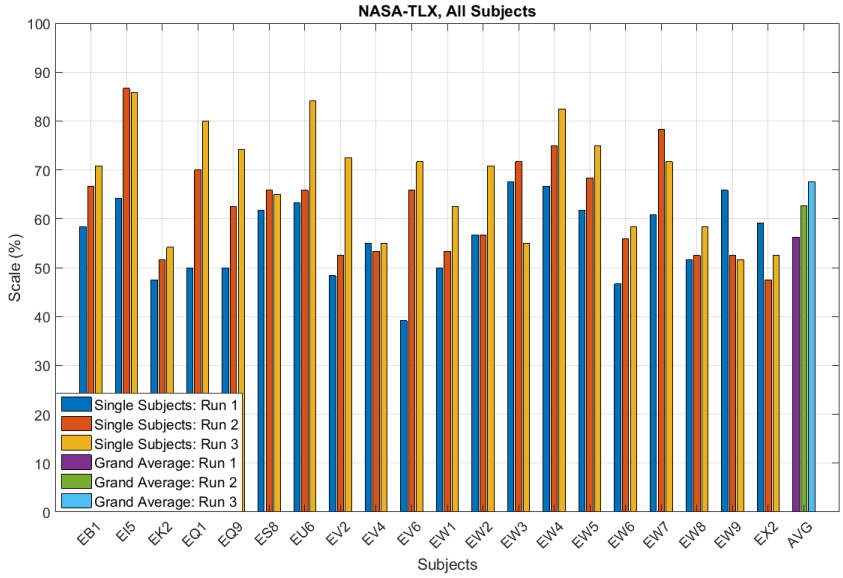

Figure 3.9: Single subject and grand average ratings according to the NASA-TLX questionnaires after runs 1, 2 and 3.

3.2.2 Behavioural Measures

The performance accuracies were calculated by the number of correctly detected target and non-target letters during a task. An accuracy of 100% means that all 5 target letters were detected correctly (by pressing the *t* key) and none of the 15 non-target letters identified as a target letter. The accuracies of each task condition were averaged over all trials at each run. The single subject and grand average performance accuracies are presented at Table 3.6. The performance accuracies decreased with increasing task difficulty (increasing *n*), which means the 1-back task yielded the highest performance accuracies (99%, 99.13% and 98.88%) and the 3-back task the lowest (88.03%, 90.84% and 89.94%). By comparing the performance accuracies between the runs however, the results show only small changes. For each task condition, there is a small increase of the performance accuracies from run 1 to run 2 and a small decrease from run 2 to run 3.

As a second performance measure, the response times of the subjects during the task execution were considered. The response time is the time difference between the letter onset and pressing the *t* key. The response times of each task condition were averaged over all trials at each run. The single subject and grand average response times are displayed at Table 3.7. The response times increased with increasing task difficulty (increasing *n*), which means that the lowest response times resulted from the 1-back task (0.53 s, 0.54 s and 0.54 s) and the highest response times from the 3-back task (0.83 s, 0.83 s and 0.76 s). Like the findings in the performance accuracies, only small changes occurred between the runs. At the 1-back task, there was a small increase from run 1 to run 3 (0.01 s), at the 2-back and 3-back task even a small decrease from run 1 to run 3 (0.06 s and 0.07 s).

Table 3.6: Single subject and grand average performance accuracies. The task conditions are averaged over all trials at each run.

Sub.	Performance Accuracy (%)								
Task	1-Back			2-Back			3-Back		
Run	1	2	3	1	2	3	1	2	3
EB1	100	96.25	99.38	95.63	96.88	95.63	85.63	88.13	90.63
EI5	95.63	98.75	94.38	97.50	98.13	94.38	80.63	87.50	82.50
EK2	100	100	100	98.75	98.75	100	95.00	96.88	96.88
EQ1	96.88	98.75	96.88	85.00	86.88	84.38	78.75	82.50	83.75
EQ9	99.38	99.38	99.38	96.88	95.00	95.63	87.50	91.25	90.00
ES8	96.88	96.88	95.63	96.88	91.88	98.13	81.88	83.13	81.88
EU6	99.38	98.75	99.38	96.88	98.75	96.25	90.00	90.00	90.00
EV2	100	100	100	98.13	99.38	98.75	93.13	96.88	93.75
EV4	99.38	100	100	93.75	95.00	96.88	87.50	94.38	93.13
EV6	100	100	100	97.50	97.50	100	90.00	93.13	87.50
EW1	100	100	100	100	98.75	100	95.63	94.38	97.50
EW2	100	99.38	98.75	96.25	99.38	100	93.75	92.50	92.50
EW3	98.75	100	100	98.75	98.75	98.13	8.75	91.25	92.50
EW4	100	97.50	100	99.38	97.50	97.50	88.75	90.63	91.25
EW5	100	100	99.38	96.88	96.88	96.25	85.63	88.75	92.50
EW6	97.50	99.38	99.38	98.13	100	97.50	91.25	96.25	90.63
EW7	100	100	100	93.75	96.25	96.88	85.00	87.50	83.13
EW8	98.13	98.13	96.25	96.88	98.75	98.75	95.63	100	93.75
EW9	98.75	99.38	98.75	98.13	98.75	99.38	83.13	85.00	86.88
EX2	99.38	100	100	96.88	97.50	96.88	83.13	86.88	88.13
AVG	99.00	99.13	98.88	96.59	97.03	97.06	88.03	90.84	89.94

Table 3.7: Single subject and grand average response times. The task conditions are averaged over all trials at each run.

Sub.	Response Time (s)								
Task	1-Back			2-Back			3-Back		
Run	1	2	3	1	2	3	1	2	3
EB1	0.64	0.58	0.61	0.67	0.66	0.61	0.87	0.82	0.66
EI5	0.62	0.64	0.64	0.76	0.90	0.90	0.89	0.92	0.91
EK2	0.53	0.46	0.45	0.56	0.53	0.52	0.66	0.67	0.58
EQ1	0.53	0.44	0.47	0.83	0.38	0.38	0.54	0.56	0.35
EQ9	0.64	0.87	1.00	0.79	0.97	1.04	1.08	1.11	1.11
ES8	0.52	0.51	0.55	0.75	0.67	0.57	0.88	0.81	0.66
EU6	0.56	0.59	0.57	0.70	0.66	0.63	0.87	0.81	0.70
EV2	0.63	0.74	0.64	0.68	0.73	0.69	0.80	0.93	0.73
EV4	0.38	0.33	0.36	0.47	0.42	0.48	0.55	0.48	0.54
EV6	0.50	0.55	0.68	0.76	0.68	0.73	0.97	0.90	0.90
EW1	0.45	0.48	0.43	0.66	0.63	0.61	0.91	0.97	0.79
EW2	0.53	0.53	0.55	0.62	0.46	0.49	0.76	0.74	0.66
EW3	0.67	0.73	0.69	0.94	0.88	0.84	0.97	1.12	1.08
EW4	0.66	0.63	0.48	0.73	0.60	0.63	0.93	0.79	0.67
EW5	0.45	0.51	0.48	0.66	0.72	0.63	0.98	0.90	0.88
EW6	0.44	0.46	0.48	0.52	0.51	0.50	0.60	0.65	0.65
EW7	0.41	0.40	0.39	0.61	0.58	0.60	0.69	0.70	0.67
EW8	0.47	0.59	0.55	0.78	0.77	0.72	0.78	0.76	0.81
EW9	0.43	0.40	0.45	0.59	0.57	0.45	1.09	1.13	1.14
EX2	0.48	0.45	0.41	0.63	0.62	0.60	0.72	0.82	0.73
AVG	0.53	0.54	0.54	0.69	0.65	0.63	0.83	0.83	0.76

3.3 MWL and MF Detection

As described in Chapter 2.5.3, the detection of MWL and MF was implemented by using the Riemannian geometry. MWL and MF were defined as too high, when the Riemannian distances of a task-run EEG reached or surpassed the threshold of the baseline EEG. The differences between the threshold and the Riemanian distances are presented at Table 3.8. The distances of each window were averaged over all trials per task condition at each run. The Riemannian distances reached or surpassed the threshold (illustrated as 0 or negative difference respectively) for 8 subjects (gray highlighted rows). 6 out of the 8 subjects belonged to the low PG, 2 to the high PG. The number of high MWL and MF detections increased with increasing experiment duration (increasing run number). 4 detections occurred at run 1, 6 at run 2 and 12 at run 3. The grand average differences of all subjects were decreasing with increasing run number (0.17, 0.13 and 0.13).

Table 3.9 shows the grand average differences for each PG separately. The differences between the threshold and the Riemanian distances of the low performers (0.15, 0.11 and 0.09) are lower than the differences of the high performers (0.18, 0.16 and 0.16). Furthermore, the differences of the low PG decreased continuously over time, whereas the differences of the high PG stayed the same during the experiment.

Table 3.8: Differences between the threshold of the baseline EEG and the Riemannian distances of the task-run EEG.

Sub.	Difference between THRS and D_R (dB)									
Run	1			2			3			PG
Task	1	2	3	1	2	3	1	2	3	
EB1	0.38	0.40	0.27	0.23	0.29	0.18	0.24	0.24	0.20	Low
EI5	0.03	0.06	0.04	0.01	**0.00**	0.03	**0.00**	0.01	**0.00**	Low
EK2	0.01	0.01	0.11	0.01	0.11	0.01	0.07	0.1	0.09	High
EQ1	0.06	0.09	0.13	**-0.04**	**-0.05**	0.08	**-0.04**	**-0.01**	0.01	Low
EQ9	0.26	0.24	0.21	0.24	0.24	0.21	0.21	0.21	0.17	Low
ES8	0.25	0.27	0.27	0.09	0.26	0.23	0.19	0.27	0.25	Low
EU6	0.41	0.40	0.35	0.37	0.34	0.28	0.32	0.38	0.34	High
EV2	0.16	0.21	0.22	0.04	0.13	0.19	0.10	0.09	0.15	High
EV4	0.21	0.20	0.20	0.21	0.20	0.22	0.21	0.22	0.22	High
EV6	**-0.02**	**-0.03**	**-0.01**	**0.00**	0.04	0.01	**-0.02**	**0.00**	**-0.02**	Low
EW1	0.22	0.21	0.22	0.16	0.19	0.19	0.14	0.13	0.12	High
EW2	0.12	0.15	0.16	0.11	0.16	0.13	0.13	0.14	0.15	High
EW3	0.13	0.16	0.13	0.01	0.04	0.01	0.01	**0.00**	**-0.03**	Low
EW4	0.09	0.09	0.10	0.10	0.10	0.09	0.08	0.08	0.08	High
EW5	0.03	0.17	0.15	0.03	0.17	0.17	**-0.01**	0.14	0.15	Low
EW6	0.04	0.03	0.05	**-0.02**	0.01	0.02	0.03	0.05	0.05	High
EW7	0.27	0.39	0.18	0.22	0.29	0.26	0.24	0.29	0.26	High
EW8	0.31	0.30	0.30	0.30	0.29	0.29	0.32	0.32	0.31	High
EW9	0.14	0.15	0.16	0.13	0.14	0.12	0.13	0.05	**0.00**	Low
EX2	**-0.02**	0.05	0.03	**-0.05**	0.04	0.02	**-0.02**	0.03	0.01	High
AVG	0.16	0.18	0.16	0.11	0.15	0.14	0.12	0.14	0.13	
	0.17			0.13			0.13			

Table 3.9: Difference between the threshold of the baseline EEG and the Riemannian distances of the task-run EEG, averaged over each PG.

		AVG differences between THRS and D_R (dB)								
PG	Run	1			2			3		
	Task	1	2	3	1	2	3	1	2	3
Low	AVG	0.14	0.17	0.15	0.08	0.12	0.12	0.08	0.10	0.08
		0.15			0.11			0.09		
High	AVG	0.17	0.20	0.18	0.14	0.17	0.16	0.15	0.17	0.16
		0.18			0.16			0.16		

4 Discussion

In order to detect increasing MWL and MF, the BP changes over time were analysed at the individual task conditions (1-back, 2-back and 3-back), ROIs (frontal, central, parietal and occipital) and PGs (high and low performers). To corroborate the findings of the BP changes, the behavioural measures (performance accuracy and response time) and subjective ratings (VAS-F and NASA-TLX questionnaires) were inspected. Furthermore, the Riemannian geometry was applied to define when the threshold of high MWL and MF was reached.

4.1 Differences between PGs and Task Conditions

The results presented in Chapter 3.1 show, that there are differences in the BP changes between the low and the high PG for both frequency bands. While for the low performers a high BP increase was elicited over time, the high performers showed only small BP increases and even BP decreases between runs. The results are supported with the estimated marginal means in Figure 3.5, where a clear separation between the two PGs can be seen with the same temporal progress as mentioned above. Furthermore, the post-hoc tests in Table 3.3 showed only a statistically significant difference at the low PG between run 1 and run 3. These findings lead to the expected assumption, that the MWL and the MF of the participants are in correlation to their task performance. Like stated from Käthner et al. [48] and Roy et al. [49], the results show that the task performance decreases with increasing MWL and MF.

Concerning the task-conditions, MWL and MF were expected to increase with increasing task difficulty. It was expected that the BP increases with

increasing n of the letter n-back task. The results in the Figures 3.1-3.4 however show, that the highest BP increase in both frequency bands was elicited at the 1-back task. A possible explanation of this outcome is, that the 1-back task was very easy to perform in relation to the other tasks, and the participants lost concentration and focus on the task. This theory can be corroborated with the BP increase at multiple, widespread cortical sites, which indicates that more cortical areas were activated during the 1-back task. Looking at Figure 3.6, it can be seen that the mean BP increase between run 2 and run 3 of the 3-back task is higher than the mean BP increase of the 1-back and 2-back task. With a longer experimental duration (additional runs) it might be possible, that the BP increase of the 3-back task surpasses the 1-back and 2-back task. The post-hoc tests in Table 3.4 revealed statistical significance for the 1-back task when comparing run 1 with run 2 and run 1 with run 3, which confirms that the 1-back task elicited the highest BP changes during the experiment. The results of the 3x3x4 repeated measures ANOVA in Table 3.1 show, that the factor *Tasks* is the only factor that showed significance in both frequency bands. The factor *ROIs* reached significance only in the theta band and the factor *Runs* only in the alpha band.

4.2 Influence of MWL and MF at the investigated ROIs

The topographical plots in the Figures 3.1 and 3.2 show that the theta BP increased at the frontal cortex for both PGs like suggested from the presented studies [45]–[47], [71]. The strongest BP increase however occurred at the parietal cortex, which does not confirm the findings of MWL increase in the presented literature. This can be explained with the overlapping BP increase towards the end of the experiment, caused by increasing MF as suggested from Boksem et al. [57] and Klimesch et al. [72]. Since the exact cortical region influenced by increasing MF is not specified in the literature, this outcome leads to the assumption that increasing MF induces a higher BP increase at the parietal cortex than at other cortical areas. The post-hoc

test comparisons at Table 3.5 revealed no statistical significance in the theta band.

The results of the BP changes in the alpha band can be observed in Figures 3.3 and 3.4. The BP decrease at the parietal sites for both PGs at run 1 supports the findings in the literature concerning MWL increase [45]–[47], [71], but there was also a BP decrease observed at frontal and central sites. In run 2, the alpha BP starts increasing at various cortical areas, which can be an indicator of increasing MF [57], [72]. This theory is confirmed by looking at the differences between the PGs in run 3: While the high performers show only small increases and even decreases in their BP, there are high BP increases in the low PG. It appears that the lower task performance of the low PG was caused by a higher MF, which is expressed by a higher alpha BP increase, especially in the fronto-central cortical areas. In contrast to the theta band, the post-hoc test comparisons in Table 3.5 revealed statistically significant differences between run 1 and run 3 for each ROI. These results show, that the influence of increasing MWL and MF is higher in the alpha band than in the theta band, which can also be seen in the topographical plots of the BP changes.

4.3 Subjective Ratings and Behavioural Measures

The outcome of the VAS-F and NASA-TLX questionnaires, illustrated in the Figures 3.8 and 3.9, states that the participants experienced an increase in their subjective workload and fatigue level and a decrease in their energy level during the experiment. Although these results indicate the influence of a cognitive demanding task on the mental state of the participants as suggested from Käthner et al. [48] and Roy et al. [49], the increases of the fatigue and workload level (and the decrease of the energy level) were expected to be higher. This can be confirmed by looking at the performance accuracies in Table 3.6: The results at a certain task condition were very similar in all 3 runs. The small increases from run 1 to run 2 can be attributed to the learning effect of the task performance, especially at the 3-back task. From run 2 to run 3, a drop in the performance accuracy was expected, but did not occur. It must be mentioned that the high task performance

accuracies resulted due to the fact, that there were only 5 targets opposed to 15 non-targets during a trial sequence. This means that detecting no target at all still leads to a performance accuracy of 75%. The same behaviour can be seen at the response times in Table 3.7: The response times for each task condition stayed the same during the experiment or even decreased, instead of increasing.

Over all, the participants experienced an increase of their fatigue and workload level, but not as high as expected. Together with the results of the behavioural measures (low increase or no increase at all), it can be said that the experiment was not demanding enough to elicit high MWL and MF in all participants. An improvement for further studies is to prolong the duration of the experiment (for example by adding another run). Since the 3-back task is already quite demanding, adding a higher n-back task to increase the difficulty of the experiment is not recommended.

4.4 MWL and MF Detection

As mentioned in Chapter 1.3, most of the pBCI systems for mental state monitoring uses various classification algorithms in order to detect high MWL or MF. The classification approach was considered for this thesis as well, in form of an LDA classifier in combination with a CSP filter based on the BP features. Due to the lack of validity and significance however, this approach was rejected.

The detection of high MWL and MF was implemented by using the Riemannian geometry. If the Riemannian distance of a task-run EEG reached or surpassed the threshold defined by the baseline EEG (expressed by 0 or negative difference values respectively), the level of MWL and MF was defined as too high. The Detection was conducted at the alpha band, because the influences of MWL and MF on the BP changes were revealed to be higher than at the theta band. The results illustrated in Table 3.8 show, that high MWL and MF was detected in 8 out of 20 participants, 6 of them belonged to the low PG. Even though the detection rate is only 40%, this outcome is quite promising. The results confirm the assumptions, that the experiment was not demanding enough for most of the participants and

that the task performance is in correlation with the MWL and MF level. Furthermore, most of the detections occurred at run 3, which approves the increase of the fatigue and workload level over time. This trend becomes even clearer when looking at the results at Table 3.9: The differences between the Riemannian distance of the task-run and the threshold are averaged over each run and divided into the two PGs. For the high PG, there is a small decrease from run 1 to run 2, from run 2 to run 3 the difference stays the same. The difference of the low PG on the contrary shows a continuous decrease during the experiment. This trend suggests, that the whole low PG would have reached their MWL and MF limit, if the experiment duration was longer.

It must be mentioned that the Riemannian distances were averaged over all trials per task condition. For an online pBCI for mental state monitoring, a single trial detection of MWL and MF is desired. A potential error source of the Riemannian geometry approach is the influence of artefacts, since the distance of an artefact influenced EEG signal also surpasses the threshold of the baseline EEG. To avoid these false positive detections, a comprehensive artefact correction must be implemented for the online pBCI system.

5 Conclusion

The aim of this thesis was to detect high MWL and MF in participants performing a cognitive demanding task in form of the letter n-back task. For the detection, the Riemannian geometry was applied on BP features of the EEG. The results of the BP changes over time partly agreed with the findings in the presented literature. For increasing MWL, the theta BP continuously increased as expected at the frontal cortex, but showed even higher increases at the parietal cortex. The alpha BP initially decreased according to the literature at the parietal cortex but also at the frontal and central areas. At run 2, the BP started to increase at multiple, widespread cortical areas. The theta and alpha BP increase towards the end of the experiment indicates increasing MF. It appears that the initial influence of increasing MWL on the BP changes gets overlapped by the influence of increasing MF. Although this behaviour was expected, it shows one of the main limitations in the thesis: A clear distinction between MWL and MF is not possible with BP features.

The results of the subjective ratings and the behavioural measures revealed another limitation of this thesis: The experiment was not cognitive demanding enough, to elicit high MWL and MF in all of the participants. This outcome was confirmed by showing high BP differences between the low and high PG. A suggested improvement for further studies is to prolong the duration of the experiment, for example by adding an additional run.

The detection of high MWL and MF by using the Riemannian distances of the task run EEG showed promising results. High MWL and MF were detected at 8 participants, 6 of them belonged to the low PG. These findings are consistent with the BP changes at both the theta and the alpha frequency band, where increasing MWL and MF was only elicited for the low PG. Additionally, the averaged differences between the Riemannian distance of

the task-run and the threshold of the low PG are continuously decreasing with increasing experiment duration.

Overall, the MWL and MF detection with the Riemannian geometry approach seems to be working. To improve this detection algorithm, future studies must be conducted with a longer experiment duration. Using this approach for an online pBCI for mental state monitoring, the next steps will be to implement a trial-wise detection algorithm and to apply an online artefact correction procedure.

Bibliography

[1] J. R. Wolpaw, N. Birbaumer, D. J. McFarland, G. Pfurtscheller, and T. M. Vaughan, "Brain-computer interfaces for communication and control," en, *Clin. Neurophysiol.*, vol. 113, no. 6, pp. 767–791, Jun. 2002.

[2] A. Kübler, B. Kotchoubey, J. Kaiser, J. R. Wolpaw, and N. Birbaumer, "Brain-computer communication: Unlocking the locked in," en, *Psychol. Bull.*, vol. 127, no. 3, pp. 358–375, May 2001.

[3] J. D. R. Millán, R. Rupp, G. R. Müller-Putz, R. Murray-Smith, C. Giugliemma, M. Tangermann, C. Vidaurre, F. Cincotti, A. Kübler, R. Leeb, C. Neuper, K.-R. Müller, and D. Mattia, "Combining Brain-Computer interfaces and assistive technologies: State-of-the-Art and challenges," en, *Front. Neurosci.*, vol. 4, Sep. 2010.

[4] J. R. Wolpaw and E. W. Wolpaw, "Brain–Computer interfaces: Something new under the sun," *Brain–Computer InterfacesPrinciples and Practice*, pp. 3–12, 2012.

[5] B. He, S. Gao, H. Yuan, and J. R. Wolpaw, "Brain–Computer interfaces," *Neural Engineering*, pp. 87–151, 2013.

[6] N. Birbaumer, N. Ghanayim, T. Hinterberger, I. Iversen, B. Kotchoubey, A. Kübler, J. Perelmouter, E. Taub, and H. Flor, "A spelling device for the paralysed," *Nature*, vol. 398, no. 6725, pp. 297–298, 1999.

[7] K.-R. Müller and B. Blankertz, "Toward noninvasive brain-computer interfaces," *IEEE Signal Processing Magazine*, vol. 23, no. 5, pp. 128–126, 2006.

[8] R. Scherer, G. R. Müller, C. Neuper, B. Graimann, and G. Pfurtscheller, "Asynchronous controlled EEG-based spelling device," *Biomedizinische Technik/Biomedical Engineering*, vol. 48, no. s1, pp. 302–303, 2003.

[9] G. R. Müller-Putz, R. Scherer, G. Pfurtscheller, and R. Rupp, "EEG-based neuroprosthesis control: A step towards clinical practice," en, *Neurosci. Lett.*, vol. 382, no. 1-2, pp. 169–174, Apr. 2005.

[10] G. Pfurtscheller, C. Guger, G. Müller, G. Krausz, and C. Neuper, "Brain oscillations control hand orthosis in a tetraplegic," *Neuroscience Letters*, vol. 292, no. 3, pp. 211–214, 2000.

[11] R. Krepki, B. Blankertz, G. Curio, and K.-R. Müller, "The berlin Brain-Computer interface (BBCI) – towards a new communication channel for online control in gaming applications," *Multimedia Tools and Applications*, vol. 33, no. 1, pp. 73–90, 2007.

[12] A. Nijholt, "BCI for games: A 'state of the art' survey," *Lecture Notes in Computer Science*, pp. 225–228, 2008.

[13] J. van Erp, F. Lotte, and M. Tangermann, "Brain-Computer interfaces: Beyond medical applications," *Computer*, vol. 45, no. 4, pp. 26–34, 2012.

[14] T. O. Zander, C. Kothe, S. Jatzev, and M. Gaertner, "Enhancing Human-Computer interaction with input from active and passive Brain-Computer interfaces," *Brain-Computer Interfaces*, pp. 181–199, 2010.

[15] T. O. Zander and C. Kothe, "Towards passive brain-computer interfaces: Applying brain-computer interface technology to human-machine systems in general," en, *J. Neural Eng.*, vol. 8, no. 2, p. 025 005, Apr. 2011.

[16] H.-J. Hwang, S. Kim, S. Choi, and C.-H. Im, "EEG-Based Brain-Computer interfaces: A thorough literature survey," *International Journal of Human-Computer Interaction*, vol. 29, no. 12, pp. 814–826, 2013.

[17] L. F. Nicolas-Alonso and J. Gomez-Gil, "Brain computer interfaces, a review," en, *Sensors*, vol. 12, no. 2, pp. 1211–1279, Jan. 2012.

[18] T. O. Zander and S. Jatzev, "Detecting affective covert user states with passive brain-computer interfaces," *2009 3rd International Conference on Affective Computing and Intelligent Interaction and Workshops*, 2009.

[19] L. George and A. Lécuyer, "Passive Brain–Computer interfaces," *Guide to Brain-Computer Music Interfacing*, pp. 297–308, 2014.

[20] D. L. Strayer and F. A. Drews, "Cell-Phone–Induced driver distraction," *Current Directions in Psychological Science*, vol. 16, no. 3, pp. 128–131, 2007.

[21] R. J. Davidse, M. P. Hagenzieker, P. C. van Wolffelaar, and W. H. Brouwer, "Effects of in-car support on mental workload and driving performance of older drivers," en, *Hum. Factors*, vol. 51, no. 4, pp. 463–476, Aug. 2009.

[22] C. Walter, W. Rosenstiel, M. Bogdan, P. Gerjets, and M. Spüler, "Online EEG-Based workload adaptation of an arithmetic learning environment," en, *Front. Hum. Neurosci.*, vol. 11, p. 286, May 2017.

[23] T. O. Zander, K. Shetty, R. Lorenz, D. R. Leff, L. R. Krol, A. W. Darzi, K. Gramann, and G.-Z. Yang, "Automated task load detection with electroencephalography: Towards passive Brain–Computer interfacing in robotic surgery," *Journal of Medical Robotics Research*, vol. 02, no. 01, p. 1 750 003, 2017.

[24] F. Putze, C. Mühl, F. Lotte, S. Fairclough, and C. Herff, *Detection and Estimation of Working Memory States and Cognitive Functions Based on Neurophysiological Measures*, en. Frontiers Media SA, Feb. 2019.

[25] A. Myrden and T. Chau, "A passive EEG-BCI for Single-Trial detection of changes in mental state," en, *IEEE Trans. Neural Syst. Rehabil. Eng.*, vol. 25, no. 4, pp. 345–356, Apr. 2017.

[26] G. Schalk and E. C. Leuthardt, "Brain-computer interfaces using electrocorticographic signals," en, *IEEE Rev. Biomed. Eng.*, vol. 4, pp. 140–154, 2011.

[27] F. Popescu, S. Fazli, Y. Badower, B. Blankertz, and K.-R. Müller, "Single trial classification of motor imagination using 6 dry EEG electrodes," en, *PLoS One*, vol. 2, no. 7, e637, Jul. 2007.

[28] S. D. Power, T. H. Falk, and T. Chau, "Classification of prefrontal activity due to mental arithmetic and music imagery using hidden markov models and frequency domain near-infrared spectroscopy," en, *J. Neural Eng.*, vol. 7, no. 2, p. 26 002, Apr. 2010.

[29] J. R. Wolpaw and C. B. Boulay, "Brain signals for Brain–Computer interfaces," *Brain-Computer Interfaces*, pp. 29–46, 2009.

[30] H. Caspers and E.-J. Speckmann, *Origin of Cerebral Field Potentials: International Symposium, Muenster, Germany*, en. 1979.

[31] S. L. Palay and V. Chan-Palay, "General morphology of neurons and neuroglia," *Comprehensive Physiology*, 2011.

[32] M. F. Bear, B. W. Connors, and M. A. Paradiso, *Neuroscience: Exploring the Brain*, en. Lippincott Raven, 2001.

[33] E. Kandel, *Principles of Neural Science, Fifth Edition*, en. McGraw Hill Professional, 2013.

[34] G. Pfurtscheller and F. H. Lopes da Silva, "Event-related EEG/MEG synchronization and desynchronization: Basic principles," en, *Clin. Neurophysiol.*, vol. 110, no. 11, pp. 1842–1857, Nov. 1999.

[35] F. H. Lopes da Silva, "Event-related potentials: General aspects of methodology and quantification," in *Niedermeyer's Electroencephalography: Basic Principles, Clinical Applications, and Related Fields, 7th edition*, F. H. Lopes da Silva and D. L. Schomer, Eds., Lippincott Williams & Wilkins, 2011, pp. 923–934.

[36] E. E. Sutter, "The brain response interface: Communication through visually-induced electrical brain responses," *Journal of Microcomputer Applications*, vol. 15, no. 1, pp. 31–45, 1992.

[37] D. Regan, *Human brain electrophysiology: evoked potentials and evoked magnetic fields in science and medicine*, en. 1989.

[38] B. Z. Allison, D. J. McFarland, G. Schalk, S. D. Zheng, M. M. Jackson, and J. R. Wolpaw, "Towards an independent brain-computer interface using steady state visual evoked potentials," en, *Clin. Neurophysiol.*, vol. 119, no. 2, pp. 399–408, Feb. 2008.

[39] D. D. Barwick, "Hans berger on the electroencephalogram of man. the fourteen original reports on the human electroencephalogram," *Journal of the Neurological Sciences*, vol. 13, no. 4, p. 507, 1971.

[40] E. Kirmizi-Alsan, Z. Bayraktaroglu, H. Gurvit, Y. H. Keskin, M. Emre, and T. Demiralp, "Comparative analysis of event-related potentials during Go/NoGo and CPT: Decomposition of electrophysiological markers of response inhibition and sustained attention," en, *Brain Res.*, vol. 1104, no. 1, pp. 114–128, Aug. 2006.

[41] L. M. Oberman, E. M. Hubbard, J. P. McCleery, E. L. Altschuler, V. S. Ramachandran, and J. A. Pineda, "EEG evidence for mirror neuron dysfunction in autism spectrum disorders," en, *Brain Res. Cogn. Brain Res.*, vol. 24, no. 2, pp. 190–198, Jul. 2005.

[42] M. A. Kisley and Z. M. Cornwell, "Gamma and beta neural activity evoked during a sensory gating paradigm: Effects of auditory, somatosensory and cross-modal stimulation," *Clinical Neurophysiology*, vol. 117, no. 11, pp. 2549–2563, 2006.

[43] C. Lalanne and J. Lorenceau, "Crossmodal integration for perception and action," en, *J. Physiol. Paris*, vol. 98, no. 1-3, pp. 265–279, Jan. 2004.

[44] G. Pfurtscheller and F. H. Lopes da Silva, "EEG Event-Related desynchronization (ERD) and Event-Related synchronization (ERS)," in *Niedermeyer's Electroencephalography: Basic Principles, Clinical Applications, and Related Fields, 7th edition*, F. H. Lopes da Silva and D. L. Schomer, Eds., Lippincott Williams & Wilkins, 2011, pp. 935–948.

[45] A. Holm, K. Lukander, J. Korpela, M. Sallinen, and K. M. I. Müller, "Estimating brain load from the EEG," en, *ScientificWorldJournal*, vol. 9, pp. 639–651, Jul. 2009.

[46] A. Stipacek, R. H. Grabner, C. Neuper, A. Fink, and A. C. Neubauer, "Sensitivity of human EEG alpha band desynchronization to different working memory components and increasing levels of memory load," en, *Neurosci. Lett.*, vol. 353, no. 3, pp. 193–196, Dec. 2003.

[47] M. W. Scerbo, F. G. Freeman, and P. J. Mikulka, "A brain-based system for adaptive automation," *Theoretical Issues in Ergonomics Science*, vol. 4, no. 1-2, pp. 200–219, 2003.

[48] I. Käthner, S. C. Wriessnegger, G. R. Müller-Putz, A. Kübler, and S. Halder, "Effects of mental workload and fatigue on the p300, alpha and theta band power during operation of an ERP (p300) brain-computer interface," en, *Biol. Psychol.*, vol. 102, pp. 118–129, Oct. 2014.

[49] R. N. Roy, S. Bonnet, S. Charbonnier, and A. Campagne, "Mental fatigue and working memory load estimation: Interaction and implications for EEG-based passive BCI," *2013 35th Annual International Conference of the IEEE Engineering in Medicine and Biology Society (EMBC)*, 2013.

[50] A. M. Owen, K. M. McMillan, A. R. Laird, and E. Bullmore, "N-back working memory paradigm: A meta-analysis of normative functional neuroimaging studies," *Human brain mapping*, vol. 25, no. 1, pp. 46–59, 2005.

[51] A. Gevins and M. E. Smith, "Electroencephalography (EEG) in neuroergonomics," *Neuroergonomics*, pp. 15–31, 2006.

[52] B. Xie and G. Salvendy, "Review and reappraisal of modelling and predicting mental workload in single- and multi-task environments," *Work & Stress*, vol. 14, no. 1, pp. 74–99, 2000.

[53] M. S. Young and N. A. Stanton, "Malleable attentional resources theory: A new explanation for the effects of mental underload on performance," en, *Hum. Factors*, vol. 44, no. 3, pp. 365–375, 2002.

[54] L. C. Thomas and C. D. Wickens, "Visual displays and cognitive tunneling: Frames of reference effects on spatial judgments and change detection," *PsycEXTRA Dataset*, 2001.

[55] B. J. Dixon, M. J. Daly, H. Chan, A. D. Vescan, I. J. Witterick, and J. C. Irish, "Surgeons blinded by enhanced navigation: The effect of augmented reality on attention," *Surgical Endoscopy*, vol. 27, no. 2, pp. 454–461, 2013.

[56] F. Dehais, M. Causse, F. Vachon, N. Régis, E. Menant, and S. Tremblay, "Failure to detect critical auditory alerts in the cockpit: Evidence for inattentional deafness," en, *Hum. Factors*, vol. 56, no. 4, pp. 631–644, Jun. 2014.

[57] M. A. S. Boksem, T. F. Meijman, and M. M. Lorist, "Effects of mental fatigue on attention: An ERP study," en, *Brain Res. Cogn. Brain Res.*, vol. 25, no. 1, pp. 107–116, Sep. 2005.

[58] G. R. Hockey, "Compensatory control in the regulation of human performance under stress and high workload; a cognitive-energetical framework," en, *Biol. Psychol.*, vol. 45, no. 1-3, pp. 73–93, Mar. 1997.

[59] A. Chaudhuri and P. O. Behan, "Fatigue and basal ganglia," en, *J. Neurol. Sci.*, vol. 179, no. S 1-2, pp. 34–42, Oct. 2000.

[60] S. A. Johnson, E. Yechiam, R. R. Murphy, S. Queller, and J. C. Stout, "Motivational processes and autonomic responsivity in asperger's disorder: Evidence from the iowa gambling task," *Journal of the International Neuropsychological Society*, vol. 12, no. 5, pp. 668–676, 2006.

[61] M. Tanaka, K. Mizuno, S. Tajima, T. Sasabe, and Y. Watanabe, "Central nervous system fatigue alters autonomic nerve activity," en, *Life Sci.*, vol. 84, no. 7-8, pp. 235–239, Feb. 2009.

[62] E. Mezzacappa, D. Kindlon, J. P. Saul, and F. Earls, "Executive and motivational control of performance task behavior, and autonomic heart-rate regulation in children: Physiologic validation of two-factor solution inhibitory control," en, *J. Child Psychol. Psychiatry*, vol. 39, no. 4, pp. 525–531, May 1998.

[63] H. Aghajani, M. Garbey, and A. Omurtag, "Measuring mental workload with EEG fNIRS," *Frontiers in Human Neuroscience*, vol. 11, 2017.

[64] S. G. Hart and L. E. Staveland, "Development of NASA-TLX (task load index): Results of empirical and theoretical research," *Advances in Psychology*, pp. 139–183, 1988.

[65] K. A. Lee, G. Hicks, and G. Nino-Murcia, "Validity and reliability of a scale to assess fatigue," en, *Psychiatry Res.*, vol. 36, no. 3, pp. 291–298, Mar. 1991.

[66] C. D. Wickens, "Multiple resources and mental workload," en, *Hum. Factors*, vol. 50, no. 3, pp. 449–455, Jun. 2008.

[67] A. Sahayadhas, K. Sundaraj, and M. Murugappan, "Detecting driver drowsiness based on sensors: A review," en, *Sensors*, vol. 12, no. 12, pp. 16 937–16 953, Dec. 2012.

[68] F. Lotte and R. N. Roy, "Brain–computer interface contributions to neuroergonomics," in *Neuroergonomics: The Brain at Work and in Everyday Life*, Elsevier, 2018, pp. 43–48.

[69] C. Tremmel, C. Herff, T. Sato, K. Rechowicz, Y. Yamani, and D. J. Krusienski, "Estimating cognitive workload in an interactive virtual reality environment using eeg," *Frontiers in Human Neuroscience*, vol. 13, 2019.

[70] F. Putze, C. Herff, C. Tremmel, T. Schultz, and D. J. Krusienski, "Decoding Mental Workload in Virtual Environments: A fNIRS Study using an Immersive n-back Task," *Proceedings of the Annual International Conference of the IEEE Engineering in Medicine and Biology Society, EMBS*, pp. 3103–3106, 2019.

[71] F. Babiloni, "Mental workload monitoring: New perspectives from neuroscience," *Proceedings of the Third International Symposium, H-WORKLOAD, Rome, Italy*, no. November, pp. 3–19, 2019.

[72] W. Klimesch, M. Doppelmayr, J. Schwaiger, P. Auinger, and T. Winkler, "Paradoxical'alpha synchronization in a memory task," *Cognitive Brain Research*, vol. 7, no. 4, pp. 493–501, 1999.

[73] Ç. İ. Acı, M. Kaya, and Y. Mishchenko, "Distinguishing mental attention states of humans via an EEG-based passive BCI using machine learning methods," *Expert Systems with Applications*, vol. 134, pp. 153–166, 2019.

[74] S. L. Klosterman and J. R. Eepp, "Investigating Ensemble Learning and Classifier Generalization in a Hybrid, Passive Brain-Computer Interface for Assessing Cognitive Workload," *Proceedings of the Annual International Conference of the IEEE Engineering in Medicine and Biology Society, EMBS*, pp. 3543–3546, 2019.

[75] N. Salimi, M. Barlow, and E. Lakshika, "Mental Workload Classification Using Short Duration EEG Data: An Ensemble Approach Based on Individual Channels," *2019 IEEE Symposium Series on Computational Intelligence, SSCI 2019*, pp. 393–398, 2019.

[76] A. Barachant, M. Congedo, C. Jutten, and C. J. M. Brain-, "Multiclass Brain-Computer Interface Classification by Riemannian Geometry To cite this version : Multi-class Brain Computer Interface Classification by Riemannian Geometry," vol. 59, no. 4, pp. 920–928, 2012.

[77] F. Yger, M. Berar, and F. Lotte, "Riemannian Approaches in Brain-Computer Interfaces: A Review," *IEEE Transactions on Neural Systems and Rehabilitation Engineering*, vol. 25, no. 10, pp. 1753–1762, 2017.

[78] A. Appriou, A. Cichocki, and F. Lotte, "Towards robust neuroadaptive hci: Exploring modern machine learning methods to estimate mental workload from eeg signals," in *Extended Abstracts of the 2018 CHI Conference on Human Factors in Computing Systems*, 2018, pp. 1–6.

[79] W. K. Kirchner, "Age differences in short-term retention of rapidly changing information," *Journal of Experimental Psychology*, vol. 55, no. 4, pp. 352–358, 1958.

[80] M. Plöchl, J. P. Ossandón, and P. König, "Combining EEG and eye tracking: Identification, characterization, and correction of eye movement artifacts in electroencephalographic data," *Frontiers in Human Neuroscience*, vol. 6, 2012.

[81] A. S. Keren, S. Yuval-Greenberg, and L. Y. Deouell, "Saccadic spike potentials in gamma-band EEG: Characterization, detection and suppression," *NeuroImage*, vol. 49, no. 3, pp. 2248–2263, 2010.

[82] R. J. Kobler, A. I. Sburlea, and G. R. Müller-Putz, "A comparison of ocular artifact removal methods for block design based electroencephalography experiments," *Proceedings of the 7th Graz Brain-Computer Interface Conference*, no. October, pp. 236–241, 2017.

[83] A. Delorme and S. Makeig, "EEGLAB: An open source toolbox for analysis of single-trial EEG dynamics including independent component analysis," en, *J. Neurosci. Methods*, vol. 134, no. 1, pp. 9–21, Mar. 2004.

[84] C. Kothe, "Lab streaming layer (LSL)," *https://github. com/sccn/labstreaminglayer. Accessed on October*, vol. 26, p. 2015, 2014.

[85] N. Retdian and T. Shima, "Power line noise suppression using n-path notch filter for EEG," *2016 International Symposium on Intelligent Signal Processing and Communication Systems (ISPACS)*, 2016.

[86] S. P. Fitzgibbon, T. W. Lewis, D. M. W. Powers, E. W. Whitham, J. O. Willoughby, and K. J. Pope, "Surface laplacian of central scalp electrical signals is insensitive to muscle contamination," en, *IEEE Trans. Biomed. Eng.*, vol. 60, no. 1, pp. 4–9, Jan. 2013.

[87] A. Barachant, A. Andreev, and M. Congedo, "The Riemannian Potato: an automatic and adaptive artifact detection method for online experiments using Riemannian geometry," *TOBI Workshop lV, Sion, Switzerland*, no. January, pp. 19–20, 2013.

[88] W. Förstner and B. Moonen, "A metric for covariance matrices," *Tech. Report of the Dpt of Geodesy and Geoinformatics, Stuttgart University*, pp. 113–128, 1999.